Rare Met. (2022) 41(4):1101–1128
https://doi.org/10.1007/s12598-021-01876-0

RARE METALS

REVIEW

MXenes nanocomposites for energy storage and conversion

Zi-Ming Qiu, Yang Bai, Yi-Dan Gao, Chun-Li Liu, Yue Ru, Ye-Can Pi, Yi-Zhou Zhang*, Yong-Song Luo*, Huan Pang*

Received: 13 July 2021 / Revised: 18 August 2021 / Accepted: 6 September 2021 / Published online: 29 November 2021

Abstract The development of two-dimensional (2D) high-performance electrode materials is the key to new advances in the fields of energy storage and conversion. As a novel family of 2D layered materials, MXenes possess distinct structural, electronic and chemical properties that enable vast application potential in many fields, including batteries, supercapacitor and catalysis. However, MXene layers are easily formed by stacking together, which significantly reduces the specific surface area, hinders the transmission of ions, and restricts other functional materials on the surface, thereby reducing performance. In addition, due to the inherent defects of a single electrode material, electrodes or catalysts made of single-phase MXene may not meet specific practical application requirements. MXenes nanocomposites materials based on enhanced electrochemical performance through nano-engineering technology and surface modification for morphological control are highly sought after to solve these challenges. This review aims to present recent advances in these emerging MXene nanocomposites for energy storage and conversion applications such as batteries, supercapacitors and catalytic reactions. We also introduced some of the challenges and opportunities in this rapidly developing field.

Keywords MXene nanocomposites; Batteries; Supercapacitors; Catalysts

1 Introduction

The ability to produce, store and use fuel for energy production shapes human society [1]. With the rapid growth of the human population, the energy demand is increasing, so is the environmental pollution problem, which requires us to develop environmentally friendly and renewable solutions to replace fossil fuels [2]. Recent advances in electrochemical energy conversion (EES) and storage technologies such as batteries [3–5], supercapacitors [6–10], and catalysis [11–16] promise alternative sources for a sustainable environment [17–19]. Although significant achievements have been made in energy storage devices, some fundamental challenges remain. For example, it is difficult for these devices to achieve high power density and high energy density at the same time [20]. Meanwhile, rechargeable energy storage is limited and comes at high costs. Therefore, it is particularly urgent and important to develop new high-performance energy storage materials to increase device performance [21–26].

Z.-M. Qiu, Y. Bai, Y.-D. Gao, C.-L. Liu, Y. Ru, Y.-C. Pi, H. Pang*
School of Chemistry and Chemical Engineering, Yangzhou University, Yangzhou 225009, China
e-mail: huanpangchem@hotmail.com; panghuan@yzu.edu.cn

Y.-Z. Zhang*
Institute of Advanced Materials and Flexible Electronics (IAMFE), School of Chemistry and Materials Science, Nanjing University of Information Science & Technology, Nanjing 210044, China
e-mail: yizhou.zhang@nuist.edu.cn

Y.-S. Luo*
Henan International Joint Laboratory of MXene Materials Microstructure, College of Physics and Electronic Engineering, Nanyang Normal University, Nanyang 473061, China
e-mail: ysluo@xynu.edu.cn

Y.-S. Luo
Key Laboratory of Microelectronics and Energy of Henan Province, Xinyang Normal University, Xinyang 464000, China

Since the discovery of graphene in 2004, two-dimensional (2D) layered materials have received more attention due to their unique physical and chemical properties [27–31]. Owing to the good electrical conductivity, high intrinsic mobility, and excellent mechanical stability of 2D nanomaterials [32], they are widely used in biology, medicine, environmental protection [33, 34], catalysis [35–38], sensors [39, 40], energy storage, and conversion [41–46]. Since then, many new 2D nanomaterials have been successfully prepared, such as phosphorene [47, 48], hexagonal boron nitrides [49–51], silicene [52, 53], transition metal dichalcogenides [54], germanane [55], and metal oxides [56, 57]. Recently, a vast family of 2D transition metal carbides and nitrides called MXenes have emerged that have shown various excellent performances [58–60]. MXenes have attracted more researchers in the field of EES due to their unique surface hydrophilicity, high conductivity, rich surface redox chemistry and superior mechanical properties. Generally, MXene is etched from the MAX phase composed of layered ternary carbides whose molecular formula are $M_{n+1}AX_n$, where M is an early transition metal (e.g., Nb, V, Ti, Ta, Zr, or Mo), A is an element from groups (Cd, Al, Si, P, S, Ga, Ge, As, In, Sn, Tl, Pb, S), and X is carbon and nitrogen. Therefore, the general formula of MXenes is $M_{n+1}X_nT_x$ (n = 1–4), T represents the surface end groups that come from the etching process. M-X atomic layers are mainly connected by ionic and covalent bonds in the MAX phase, while metallic bonds connect M-A layer [61]. In general, the covalent bonds are greater than the ionic bonds, and the ionic bonds are greater than the metal bonds; thus, the M-A binding force connected by the metal bond is relatively weak, which provides favorable conditions for etching the A layer from the MAX phase (Fig. 1) [62].

So far, among all discovered MXene, Ti_3AlC_2 is the most widely studied [63–65]. The key to obtaining Ti_3C_2 material is to precisely etch the Al atomic layer in Ti_3AlC_2 taking advantage of the etchant's high selectivity. The etchant widely used to prepare Ti_3C_2 is usually hydrofluoric acid (HF) [66]. After the Al atomic layer etched accurately, the ion or solvent water continues to react with the surface of the layered material to form the surface functional group –OH, –F, or –O, which is denoted as $Ti_3C_2T_x$, where the functional group –F, –OH, or –O is represented as T_x. Because these surface functional groups –OH, –F, or –O are hydrophilic, they can easily form hydrogen bonds with water to form a stable colloidal solution. By controlling the synthesis conditions, the surface functional groups can be adjusted. However, this method of first etching and then stripping into a single layer or several layers does not lead to high yields. This is because during the peeling process, the exposed metal sites on the surface are easily oxidized in the air, and the electrical conductivity of the $Ti_3C_2T_x$ material is reduced. Other etchants such as NH_4F/NH_4HF_2, HF/LiCl, KCl/HF salt solution, LiF, and HCl were tried to solve the above problems, improving the efficiency and safety of the experiment [67–73]. The cation is in a free state during the etching process, and the inserted water molecules and cations in the MX layer can enlarge the spacing of the $Ti_3C_2T_x$ material. Mild shaking can be used to obtain single-layer or multi-layer $Ti_3C_2T_x$. To improve MXenes materials' performance, the surface terminating functional groups or intercalation ions are sometimes adjusted to achieve changes in the energy band and the interlayer spacing. Besides, methods commonly used to prepare MXenes include fluoride salt, chlorine, and other high-temperature corrosion and chemical vapor deposition [74–79]. However, it is necessary to strictly control the time, temperature, atmosphere and other conditions. Since the Al layer in the $Ti_3C_2T_x$ material is removed by etching, its electrical conductivity is reduced. Like other 2D materials, the layers are stacked together because of the interaction between the electrode layers, the structure becomes very compact, and the specific surface area is also greatly reduced [80, 81]. This will reduce the number of active surface sites [82, 83], block the transmission of electromagnetic waves and ions [84], and also prevent it from loading other functional materials, resulting in poor performance [85]. Owing to the shortcomings of single electrode materials, the electrodes or catalysts made from them have poor performance [86, 87]. Accordingly, researchers have tried to incorporate other materials into the MXene layer, and develop composite materials with high electrochemical properties through morphological control through nano-engineering and surface modification technologies [88–95].

This review aims to introduce the latest development of emerging MXene-based nanocomposites material in energy storage and conversion applications. Some applications of MXene nanocomposites in batteries, supercapacitors and catalytic reactions are presented. The main challenges and prospects of MXene nanocomposite materials in the future energy conversion and storage are also put forward. The structure of this review is shown in Fig. 2 [96–103].

2 Batteries

Traditional non-renewable energy resources (such as oil and coal) on the earth are gradually depleting; meanwhile, the large-scale exploitation and use of conventional energy have caused severe environmental pollution [104–106]. Therefore, vigorous research efforts have been devoted to developing sustainable and clean energy resources such as solar energy, tidal energy, wind energy, and high-efficiency

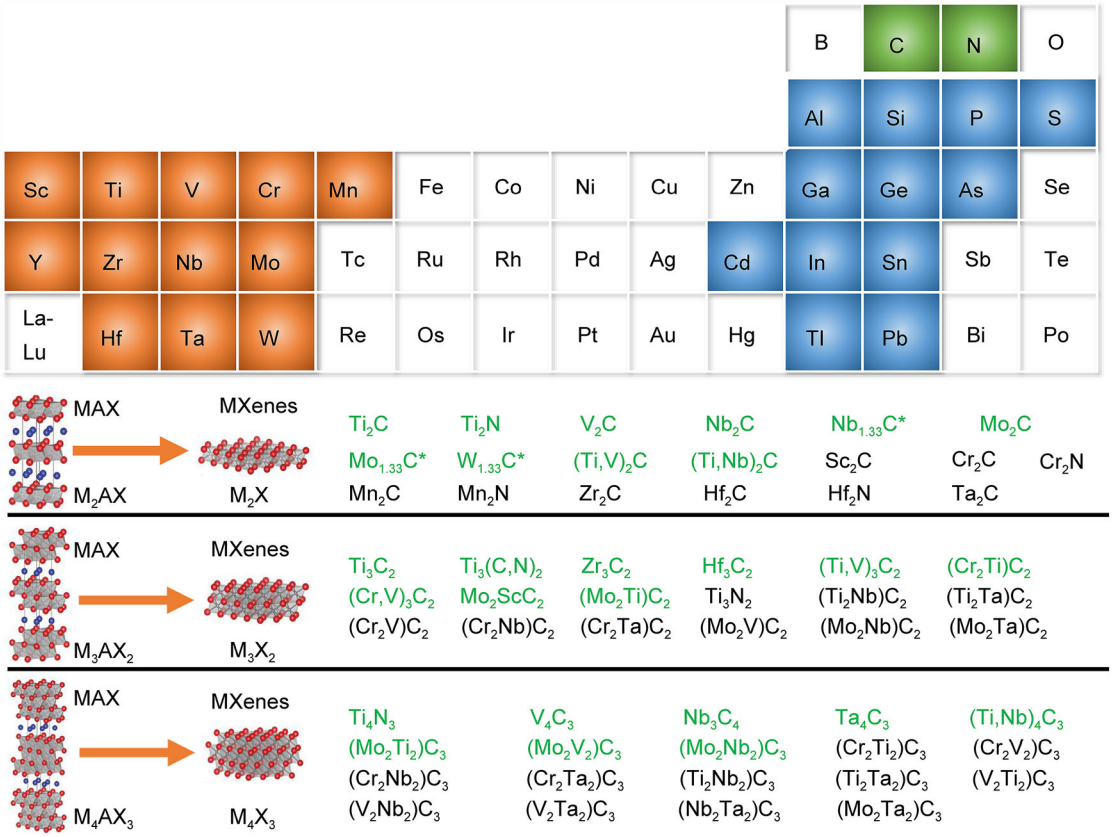

Fig. 1 MAX and MXene genomes: with combinations of 12 transition metals (orange), 12 group A elements (blue), and 2 X elements (green), close to 100 MAX phases that have either M_2AX, M_3AX_2, or M_4AX_3 structures that have been reported to date. Moreover, transition metals in M layer can form a solid solution and/or double-M ordered phases, leading to numerous complex multi-elemental phases. By selective etching of A layer from MAX phases, close to 30 MXenes have been experimentally synthesized (marked in green) and many more are theoretically predicted. The asterisks indicate MXenes with ordered divacancies. Reproduced with permission from Ref. [62]. Copyright 2017, Royal Society of Chemistry. Reproduced with permission from Ref. [63]. Copyright 2018, Wiley–VCH

batteries to reduce the consumption and dependence on traditional energy sources [107, 108]. Among them, rechargeable batteries have attracted heated attention due to their long cycle life, short charging time, and mobility. To further improve the performance, the preparation of new electrode materials becomes particularly important [109].

2.1 Li-ion batteries

Li-ion batteries are widely used in various portable electronic devices due to their long cycle life, high energy density and environmental friendliness. It is urgent to improve the current LIB's energy density and rate capability [58, 110–116]. MXenes have been studied to meet this challenge due to their adjustable surface functional groups, inherent high metal conductivity, embedding ability, and excellent mechanical stability [117–121].

Silicon and silicon-based anodes have attracted widespread attention due to their abundant reserves and large specific capacity. However, due to the inherent poor conductivity, the inevitable volume expansion during the lithium insertion process, and the irreversible formation of Li silicate and Li_2O in the first cycle, the cycle life, initial coulombic efficiency (CE) and the rate performance of the silicon-based anode are poor. Very recently, Meng et al. [122] reported a new method for preparing $Ti_3C_2T_x$ scrolls by cold quenching in liquid nitrogen. High-capacity silicon nanoparticles were added during the preparation process to generate $Ti_3C_2T_x$/Si composite scrolls in situ. The addition of 10% silicon nanoparticles greatly improves the capacity, rate capability and cycle stability of $Ti_3C_2T_x$ scrolls. Wei et al. [123] prepared SiO/wrinkled MXene composites through a simple and scalable electrostatic self-assembly method. Under the action of folds MXene, it can be more tightly coupled with SiO particles to avoid electrical isolation of active materials due to volume expansion, and it can also improve the inherent low conductivity of SiO, so that the SiO/wrinkled MXene composite material exhibits excellent electrochemical performance.

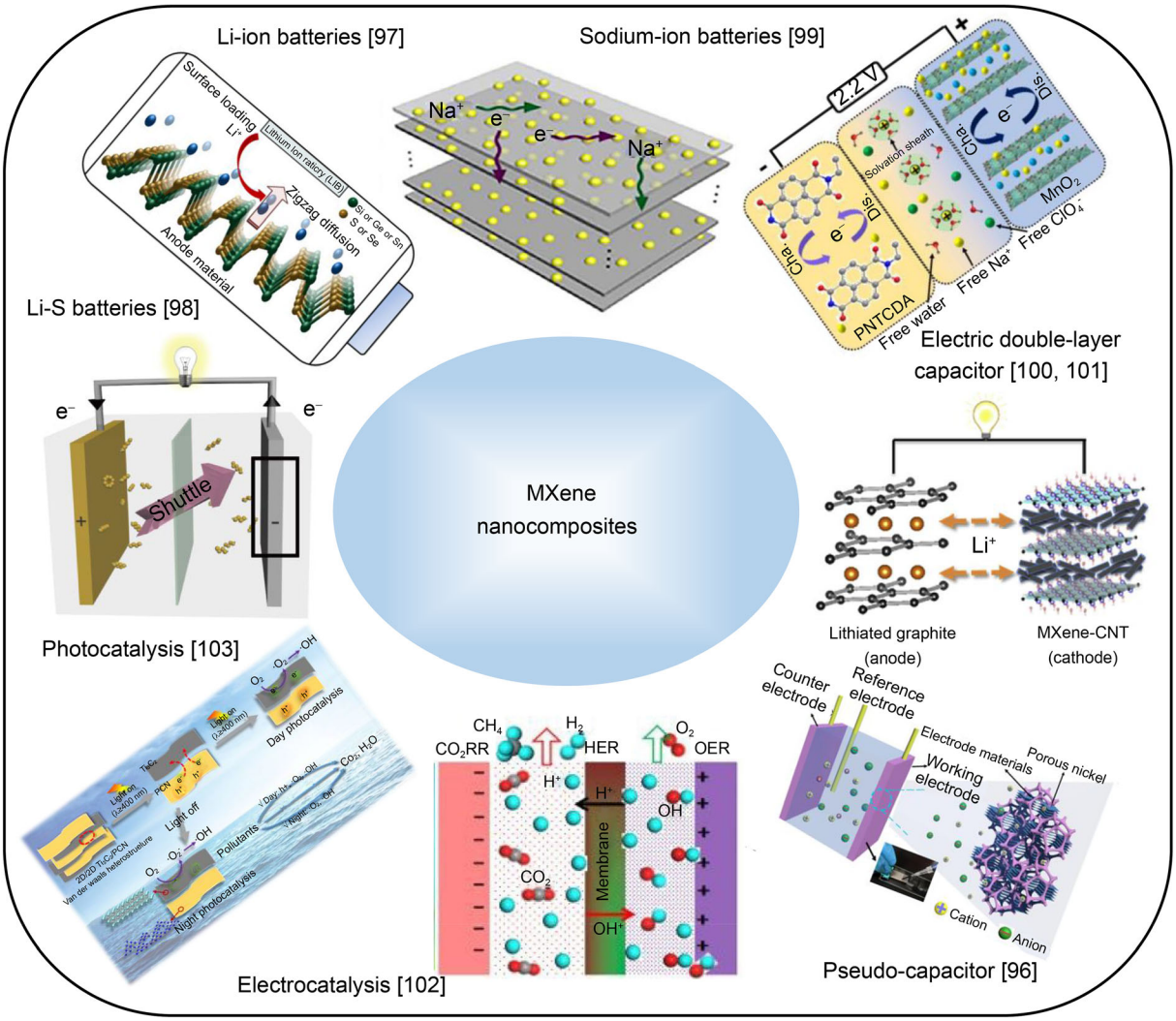

Fig. 2 Schematic diagram of MXenes composites for energy conversion and storage

Mu and colleagues [125] designed and synthesized SiO_2/MXene microspheres for the first time by combining spray drying with the Stöber method (Fig. 3a). First, HF acid was used to selectively etch the Al layer in the MAX phase to prepare laminated MXenes ($Ti_3C_2T_x$). Then, SiO_2 nanoparticles produced by the hydrolysis of TEOS were grown on the MXene sheet. Owing to the binding effect between the MXene matrix and the SiO_2 nanoparticles, the SiO_2 nanoparticles can be firmly anchored on the MXene sheet. Finally, SiO_2/MXene microspheres were prepared by the spray-drying method. The inside of the microsphere is a stacked MXene-SiO_2-MXene laminate structure, and a flexible MXene film wraps the outside of the microsphere [124, 125]. Through bonding, SiO_2 nanoparticles are firmly fixed on the microspheres composed of laminated MXene. And this structure has synergistic effects: (1) the sandwich MXene matrix inhibits the agglomeration of SiO_2 nanoparticles, while the embedded SiO_2 nanoparticles can prevent the re-stacking of MXene flakes; (2) multilayer MXene with a three-dimensional (3D) network has high metallic conductivity, which can promote the transfer of electrons and facilitate the diffusion of lithium-ions; (3) because the tough MXene film covers the surface of the microspheres, the specific surface area and the occurrence of side reactions are significantly reduced, and the CE is improved; (4) because of the bonding between the MXene matrix and the SiO_2 nanoparticles, the entire microsphere structure is more stable; (5) SiO_2 will have large volume changes during the cycle, and the flexible MXene matrix can effectively alleviate the strain caused by it; (6) SiO_2 nanoparticles with size of about 30 nm can shorten the lithium ions' path length, effectively avoiding lithium-ions from breaking. Therefore, the microsphere SiO_2/MXene hybrid material exhibits excellent electrochemical performance as the anode in LIBs. For example, at 100 $mA{\cdot}g^{-1}$, it has a high reversible capacity of 838 $mAh{\cdot}g^{-1}$, which

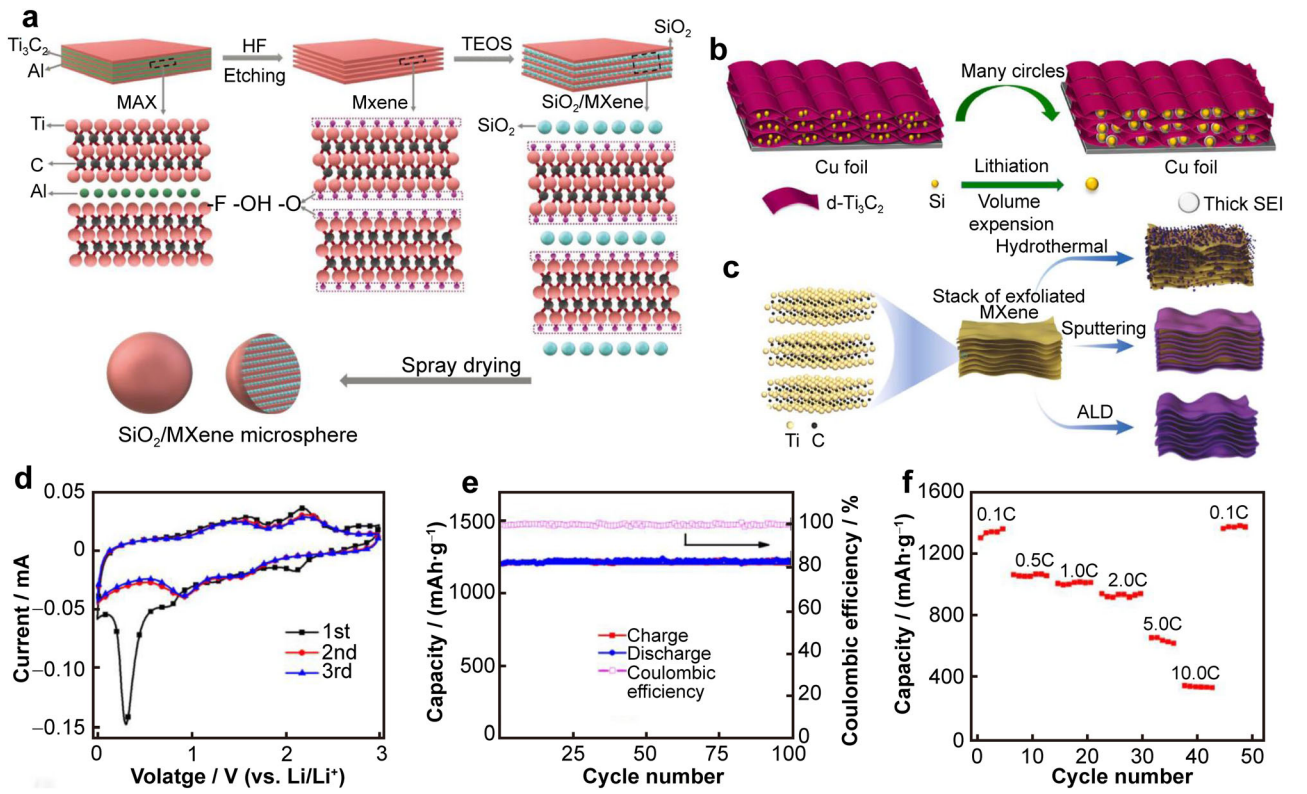

Fig. 3 **a** Schematic diagram for synthesis process of SiO_2/MXene microspheres. Reproduced with permission from Ref. [125]. Copyright 2019, Wiley–VCH. **b** Illustration of sandwich-like Si/d-Ti_3C_2 hybrids as an electrode of LIBs: electrochemical response of spray-coated $Ti_3C_2T_x$/$NiCo_2O_4$ films ($m(NiCo_2O_4)/m(Ti_3C_2T_x)$ = 1) vs. Li/Li^+. Reproduced with permission from Ref. [128]. Copyright 2017, Elsevier. **c** Schematic illustration of various methods used for SnO_2 deposition on Ti_3C_2 MXene sheets, including hydrothermal synthesis, sputtering, and ALD, where an atomistic view of exfoliated MXene sheets is shown on left, stack of exfoliated MXene sheets is in middle, and MXene hybrid electrodes after SnO_2 deposition are on right. Reproduced with permission from Ref. [126]. Copyright 2019, Elsevier. **d** CVs at 0.1 $mV·s^{-1}$; **e** cycling performance of activated sample at 1.0C; **f** rate performance. Reproduced with permission from Ref. [137]. Copyright 2016, Elsevier

has high reversible capacity and excellent cycle stability. At 200 $mA·g^{-1}$, the capacity retention rate is 97% in 100 cycles. The capacity retention rate in 200 cycles at 1 $A·g^{-1}$ reaches 93%. Significantly, when the mass load is 2.58 $mg·cm^{-2}$, the area capacity of the SiO_2/MXene anode is as high as 2.16 $mAh·cm^{-2}$ [46].

There are relatively few researches on applying Si/MXene hybrid materials as LIBs anodes. Zhu et al. [126] prepared a porous, sandwich-like Si/d-Ti_3C_2 hybrid in a synthetic approach, as shown in Fig. 3b. This hybrid material has high electrochemical cycle stability; even after 200 cycles, the reversible capacity of Si/d-Ti_3C_2 can reach more than 1130 $mAh·g^{-1}$. First of all, d-Ti_3C_2 can effectively alleviate the volume expansion during the lithiation process; secondly, it can also increase the electrical contact between the electrode frame and the silicon nanoparticles.

It is known that there are surface functional groups on the surface of MXene nanosheets, such as –O, –OH or –F [42, 111]. These surface functional groups provide hydrophilicity, which is beneficial for contacting aqueous electrolytes but may be harmful to contact non-aqueous electrolytes. The adsorption and insertion of metal ions are controlled by chemical properties and surface structure to achieve the best working potential window and storage capacity. Therefore, to improve its electrochemical performance in organic electrolytes, decoration of MXene surface through chemical treatment can be used. For example, based on density functional theory calculations, researchers predicted that the theoretical capacity of exposed Ti_3C_2 to embed Li is 320 $mAh·g^{-1}$, and it can be doubled when a double layer of Li atoms is formed between MXene sheets [58, 127]. However, functional groups such as –OH or –F on the surface of MXene limits the capacity of Li-ions. Therefore, the lithium-ion storage capacity of $Ti_3C_2F_2$ is only 130 $mAh·g^{-1}$, and the lithium-ion storage capacity of $Ti_3C_2(OH)_2$ is 67 $mAh·g^{-1}$ [43].

Subsequently, Ahmed et al. [128–130] used a hydrothermal synthesis method to deposit SnO_2 on the peeled MXene sheets and then used sputtering or atomic layer deposition (ALD) deposition to grow MXene film on the copper foil substrate. Figure 3c shows a schematic diagram of three different synthesis processes and their

effects on MXene sheets. The hydrothermal synthesis method allows SnO_2 particles to form on the twisted MXene flakes under high pressure, high temperature and water environment, so that MXene is modified. The MXene sheet is covered with the SnO_2 thin film deposited by sputtering, mainly on the accessible outer surface, while MXene retains its morphology and structure due to the non-conformity of the sputtering process. The emergence of the ALD process allows the conformal SnO_2 film to cover the surface of MXene completely. The research showed that during the cycling of lithium-ion batteries (LIBs), MXene could be prepared by ALD to make it stably loaded with SnO_2 anode [131, 132]. Simultaneously, because the oxidants commonly used in ALD will cause harmful oxidation of MXene at high temperatures, the surface functional groups of MXene can protect it from this oxidation, which acts as good protection for MXene. The designed SnO_2/MXene electrode provides high capacity because SnO_2 has a conversion reaction. The MXene sheet provides a conductive network to adapt to the significant volume changes of SnO_2 during battery charging-discharging. Under the same conditions, if a thin HfO_2 passivation layer is deposited on the surface of SnO_2, the performance of the SnO_2/MXene electrode will be further improved, and the stable specific capacity of the electrode is 843 $mAh{\cdot}g^{-1}$. The presence of the HfO_2 layer will slow down the reaction between SnO_2 and the electrolyte, and the crystal structure of SnO_2 will not change during the cycle [128].

Because of the electrostatic interaction between metal cations and Ti_3C_2 MXene, Zhang et al. [133] successfully synthesized ultra-thin, curved, wrinkled and larger interlayer spacing NiCo-LDH nanosheets on the surface of Ti_3C_2 MXene. NiCo-LDH is tightly anchored on the surface of Ti_3C_2 MXene, which greatly enhances the durability of the structure. The unique microstructure of NiCo-LDH exposes more active sites, which is conducive to the diffusion of lithium ions inside the active material. In the process of lithium-ion insertion, the layered NiCo-LDH/Ti_3C_2 MXene can greatly reduce the volume expansion.

It is an attractive idea to develop high-performance, multifunctional materials for applications in energy conversion and storage, catalysis, etc., through a well-designed approach with complementary properties of nanomaterials. For example, researches used alternating filtration, spraying, and in-situ wet chemical synthesis to hybridize $Ti_3C_2T_x$ and transition metal oxides (TMOs), such as $NiCo_2O_4$ and Co_3O_4. By successfully combing the metal conductivity of $Ti_3C_2T_x$ with the high capacity of TMOs, excellent electrochemical performance was obtained on an anode of LIBs [134–137]. The thus-obtained MXene/TMO composite membrane electrode has a high reversible capacity exceeding 1200 $mAh{\cdot}g^{-1}$. The excellent rate performance and long-term stability exhibited by all films are unexpected. In particular, the reversible capacity of the coated $Ti_3C_2T_x/NiCo_2O_4$ composite film electrode at 0.1, 5 and 10 °C are 1330, 650 and 350 $mAh{\cdot}g^{-1}$, respectively, and there is no capacity degradation after hundreds of cycles (Fig. 3d–f) [128].

2.2 Sodium-ion batteries

Owing to the lithium sources and uneven distribution of lithium, researchers have begun to pay attention to the development of new low-cost non-lithium rechargeable batteries. Sodium is another alkali metal whose physical and chemical properties are similar to lithium. Moreover, its low cost, wide distribution, and rich resources have made it an excellent EES candidate. Therefore, sodium-ion batteries have the potential to become the next generation of energy storage batteries [99, 128, 138–141].

MXene materials have great application prospects in sodium-ion batteries because of their excellent properties. This application's main challenge is the limited ion accessibility between the multilayer MXene layers, resulting in poor cycle life and low capacity [142, 143]. To overcome this, researchers have tried to apply a method that has been successfully used to increase the interlayer spacing of clays: pillaring (that is, inserting a second species between layers) in MXenes. Recently, Maughan et al. [144] successfully inserted silicon-based pillars between Ti_3C_2 layers through a new amine-assisted columnization method. Figure 4a is a schematic diagram of the synthesis process of columnar MXene. Ghidiu et al. [145] used HCl and fluoride salts to etch the MAX phase and washed the synthesized Ti_3C_2 with hydrochloric acid to remove impurities to obtain Ti_3C_2-OH. To insert Si (Ti_3C_2-OH-Si) between Ti_3C_2 layers, Ti_3C_2-OH was mixed with DDA and TEOS and calcined at 300, 400, or 500 °C under argon. The interlayer spacing can be controlled by changing the calcination temperature and selecting amines, and the maximum interlayer spacing reported by MXene could reach 3.2 nm. The Pillaring method can also increase the surface area; as shown by the Brunauer Emmett Teller (BET) result, the surface area reached 235 $m^2{\cdot}g^{-1}$, 60 times the original surface area. This is also the highest reported surface area of MXenes obtained using the intercalation method. Simultaneously, the surface chemistry can be optimized for the pillaring process according to the intercalation mechanism. Researchers tested the porous MXene in sodium-ion battery applications. It has more excellent capacity, better stability and rate performance, and maintains a 98.5% capacity between the 50th and 100th cycles. This shows that the pillar support technology is of great help in applying MXenes materials in sodium-ion batteries through improving MXenes nanocomposites'

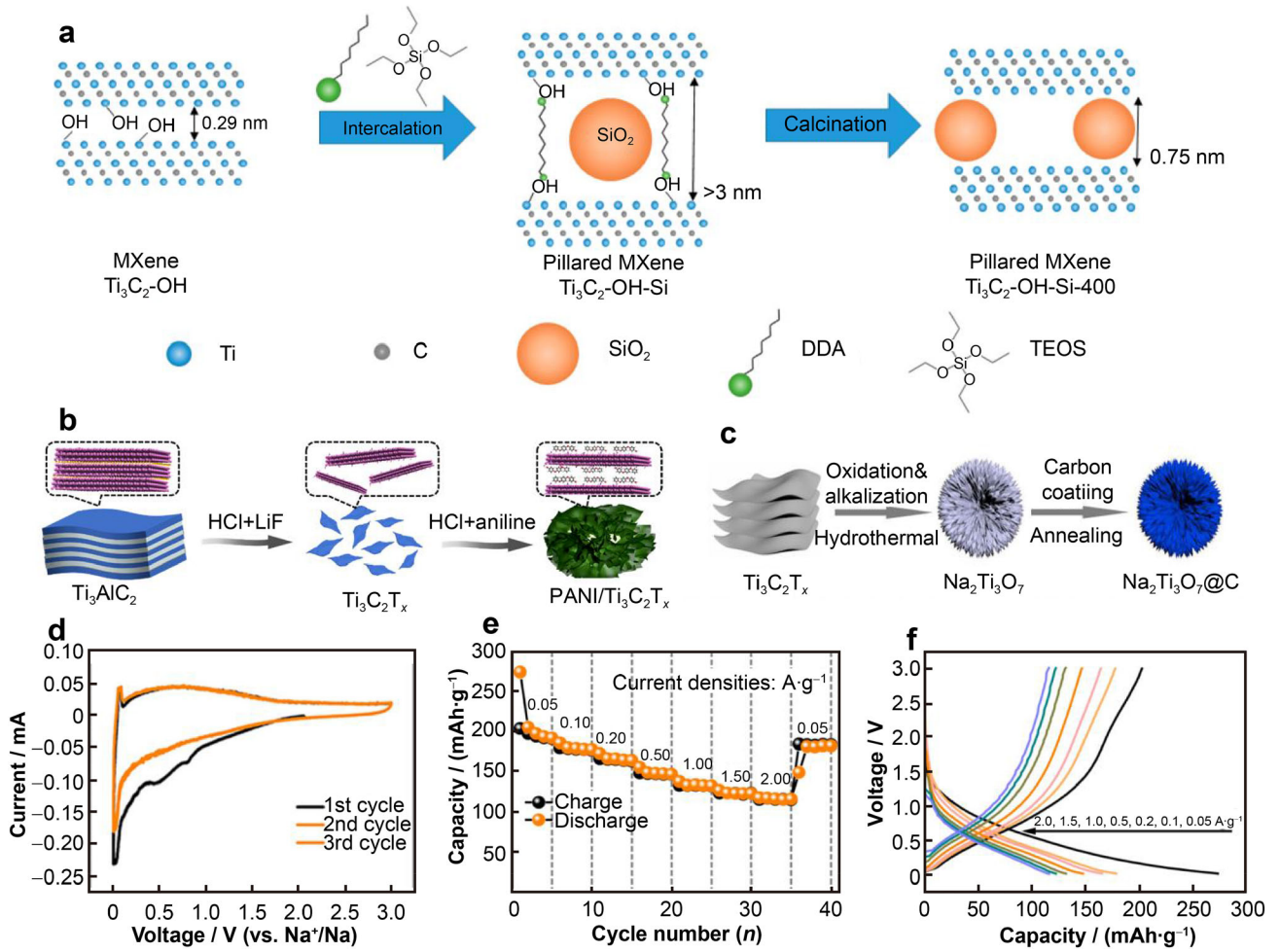

Fig. 4 **a** Schematic diagram illustrating pillaring process of MXenes; **b** schematic diagram showing formation process of 3D PANI/$Ti_3C_2T_x$ network by self-assembly method. Reproduced with permission from Ref. [145, 145] Copyright 2020, American Chemical Society. **c** Illustration of route for synthesis of $Na_2Ti_3O_7$@C, electrochemical measurements of $Na_2Ti_3O_7$@C composite in sodium-ion batteries; **d** CV curves at a scan rate of 0.1 $mV{\cdot}s^{-1}$; **e–f** rate performance and corresponding charge/discharge curves. Reproduced with permission from Ref. [151]. Copyright 2019, Elsevier

performance and contributing to the future application of MXene nanocomposites.

The functional groups on the surface of MXene are negatively charged and can anchor sodium ions, resulting in slow ion diffusion kinetics. To overcome this, Chen et al. [146] and Wang et al. [147] designed a positively charged conductive polyaniline (PANI) and $Ti_3C_2T_x$ to self-assemble into a 3D PANI/$Ti_3C_2T_x$ network. The preparation process (Fig. 4b) is mainly through self-assembly, and the conductive polymer PANI is used to construct a layered porous 3D PANI/$Ti_3C_2T_x$ network. First, the Ti_3AlC_2 suspension was obtained using a LiF-HCl aqueous solution. The polymerization was conducted by slowly adding 1 $mol{\cdot}L^{-1}$ aqueous HCl solution containing a certain amount of aniline monomer to the $Ti_3C_2T_x$ suspension under ice bath conditions. In this process, the aniline monomer may first be adsorbed to $Ti_3C_2T_x$ through electrostatic interaction as the zeta potential and hydrogen bond prove that their charges are opposite. Subsequently, the aniline monomer polymerizes along the surface and bridges adjacent $Ti_3C_2T_x$ nanosheets, and finally forms a 3D PANI/$Ti_3C_2T_x$ network.

The introduced polymers (polyaniline) induce the assembly of $Ti_3C_2T_x$ nanosheets and increase the interlayer spacing of $Ti_3C_2T_x$ nanosheets due to the intercalation effect. Studies have proved that the 3D network of $Ti_3C_2T_x$ with PANI has good sodium storage performance compared with other $Ti_3C_2T_x$ components. The reasons are summarized as follows: (1) unique 3D network structure and expanded interlayer spacing for the Na-ion, which can improve the kinetics. (2) there is a covalent Ti-N bond at the interface between $Ti_3C_2T_x$ and PANI, which significantly enhances the durability of the structure; (3) the PANI/$Ti_3C_2T_x$ nanosheet surface is positively charged,

which substantially accelerates the transfer of Na^+; (4) PANI/$Ti_3C_2T_x$ has high conductivity, and the charge transfer resistance has been greatly reduced, which helps fast electron transfer. Because of the above reasons, PANI/$Ti_3C_2T_x$ has a high specific capacity, which is better than those of PANI (14.8 mAh·g^{-1}), $Ti_3C_2T_x$ (89.2 mAh·g^{-1}) and HCl/$Ti_3C_2T_x$ (123 mAh·g^{-1}), at 100 mA·g^{-1}. It has a high specific capacity of 254 mAh·g^{-1} at 100 mA·g^{-1}, and it also has excellent high-rate cycle life (> 10,000 times). PANI/$Ti_3C_2T_x$ exhibits excellent performance even when operating under severe temperature range from + 50 to − 30 °C.

Multilayer $Ti_3C_2T_x$ material has a relatively low specific capacity, which limits its practical application [148, 149]. Tao et al. [150] and Zhong et al. [151] recently prepared a pompons-like composite material $Na_2Ti_3O_7$@C through MXene derivatives and applied it as anode electrode material for sodium ions. Figure 4c is a schematic diagram of the synthesis process of $Na_2Ti_3O_7$@C. First, $Ti_3C_2T_x$ can be obtained by selective etching of Ti_3AlC_2, because the functional groups (–OH, –O, –F) on $Ti_3C_2T_x$ have an opposite adsorption effect on Na-ions in the solution, followed by mixing the product with a certain amount of hydrogen peroxide and sodium hydroxide. Then through the hydrothermal reaction, the staggered $Na_2Ti_3O_7$ nanoribbons can be generated in situ. Then it is dispersed in the Tris buffer solution, and at the same time, dopamine hydrochloride is quickly added to the suspension to form a dopamine-coated $Na_2Ti_3O_7$ precursor. To obtain the final product $Na_2Ti_3O_7$@C, the precursor needs to be gently annealed. Therefore, a simple hydrothermal method and an economically feasible and measurable annealing process were used to prepare $Na_2Ti_3O_7$ nanobelts. The surface of the $Na_2Ti_3O_7$ nanobelt is evenly coated with carbon. In this way, by synthesizing cross-linked nanobelts with open porosity and proper interlayer spacing $Na_2Ti_3O_7$@C, the structural stability and slow sodium ion reaction kinetics can be greatly improved. Simultaneously, the surface is covered with a uniform carbon coating, which can effectively improve the conductivity, promote electron transport, and maintain the structure's integrity during cycling. When $Na_2Ti_3O_7$@C is used as the negative electrode material of sodium-ion batteries, it has excellent electrochemical performance. Its reversible capacity is as high as 173 mAh·g^{-1} at 200 mA·g^{-1}; its cycle life can be up to 200, with each cycle attenuation being only 0.026%. In the first cathode process, two broad peaks around 0.45 and 0.80 V form, corresponding to the decomposition of the electrolyte and the formation of a solid-phase electrolyte interface layer. $Na_2Ti_3O_7$@C has high conductivity and fast reaction kinetics, and its reversible capacities are 115, 123, 131, 146, 165, 177, and 195mAh·g^{-1}. When the current density is restored to 0.05 mA·g^{-1}, $Na_2Ti_3O_7$@C can still output a reversible capacity of 183 mAh·g^{-1} in the subsequent cycles. At the same time, its curves almost overlap with good reproducibility, showing that the electrochemical properties of $Na_2Ti_3O_7$@C are highly reversible (Fig. 4d–f) [137].

2.3 Lithium-sulfur batteries (LSBs)

LSBs are deemed a promising development direction of the next-generation high-energy rechargeable lithium batteries because of their high theoretical energy density and low cost. However, LSBs have inherent disadvantages, such as low specific capacity, low energy efficiency, and rapid capacity decay. These problems are mainly caused by the inevitable shuttle effect of lithium polysulfides (LiPSs) intermediates, the large volume change of the sulfur electrode during the cycle, and the poor conductivity of sulfur [152–156].

The strong adsorption of transition metal disulfides and metal oxides on polar materials or the physical constraints of LiPSs in nanostructured carbon composites, have attracted more and more attention from researchers. However, even if it has chemical adsorption and physical constraints, their effect on improving battery performance is limited [157]. For example, Jiao et al. [158] immobilized polysulfide by anchoring uniformly dispersed TiO_2 on the MXene nanosheet as a capture center. The heterostructure of TiO_2-Mxene has a large surface area, high efficiency in capturing polysulfide, high electrocatalytic activity and conductivity advantage. This catalyst can effectively improve cycle stability and sulfur utilization in lithium-sulfur batteries. Alhabeb et al. [159] and Huang et al. [160] synthesized TiS_2 nanosheets confined by N, S co-doped porous carbon (TiS_2@NSC) by coating polydopamine (PDA) on $Ti_3C_2T_x$ (Fig. 5a). Inspired by the adhesion of proteins, some researchers have used PDA for the surface functionalization and modification of materials, which can easily adsorb a kind of dopamine (DA) through self-polymerization on various substrates. Introducing PDA to the surface of MXene can protect $Ti_3C_2T_x$ nanosheets from re-stacking and oxidation. Also, PDA-derived carbon will limit TiS_2 during the vulcanization process, and its product is TiS_2@NSC. When the main sulfur body uses TiS_2@NSC, the corresponding sulfur cathode (S/TiS_2@NSC, 70 wt% sulfur, 2.5 mg·S·cm^{-2}) can reach 920 mAh·g^{-1} in 120 cycles at 0.2C. After 200 cycles at 1.0C discharge capacity, the specific capacity can reach 695 mAh·g^{-1}, the electrolyte (μl)/sulfur (mg) ratio (E/S) is 6. Simultaneously, as a stand-alone electrode, by integrating TiS_2@NSC with cotton carbon fiber (CF), after 100 cycles under the condition of an E/S of 8 at 0.1C, a high area capacity is maintained.

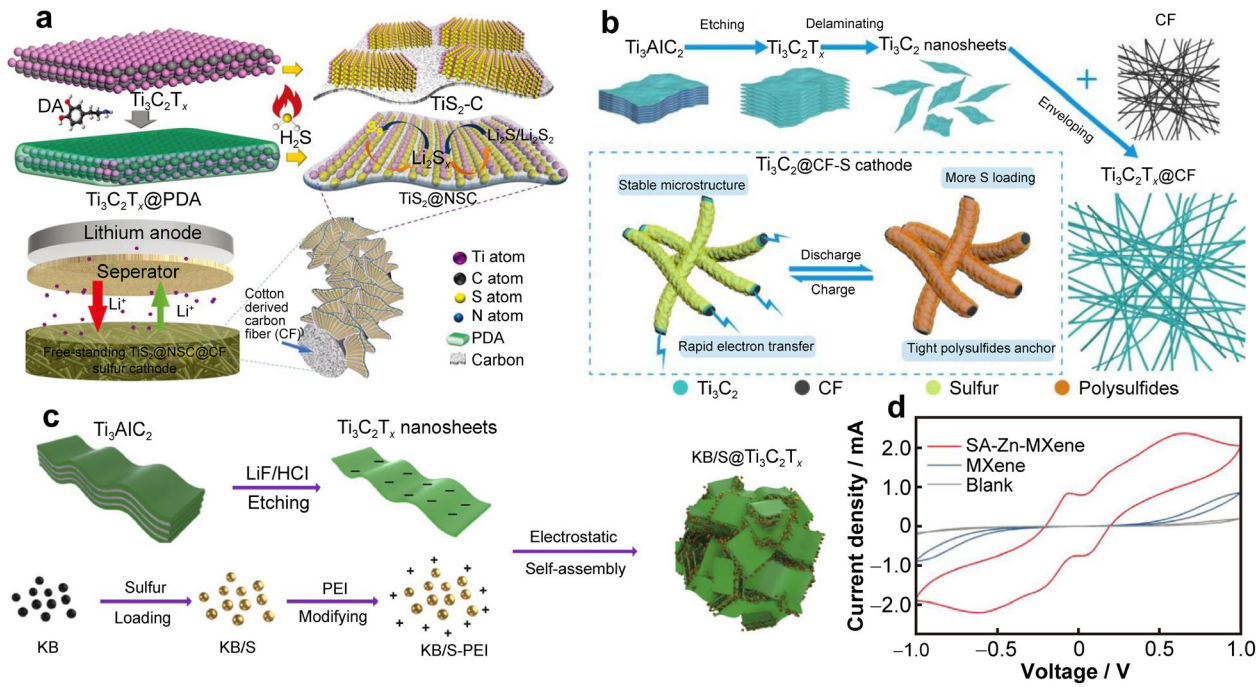

Fig. 5 **a** Schematic illustration of synthesis of sandwich-like, single-layer TiS_2 nanosheets confined within PDA derived N, S codoped porous carbon (TiS_2@NSC), and its application in LSBs as a bifunctional sulfur host for trapping LiPSs and catalytically accelerating conversion of LiPSs. Reproduced with permission from Ref. [160]. Copyright 2019, WILEY–VCH. **b** Schematic illustration of Ti_3C_2@CF preparation and as a multifunctional cathode material to ameliorate performance of Li–S batteries. Reproduced with permission from Ref. [161]. Copyright 2020, Royal Society of Chemistry. **c** Schematic illustration of fabrication of KB/S@$Ti_3C_2T_x$ composite. Reproduced with permission from Ref. [164]. Copyright 2020, Springer. **d** CVs of SA-Zn-MXene, MXene, and Al foil from −1.0 to 1.0 V at 3 mV·s^{-1}, revealing efficient catalytic effect of SA-Zn-MXene. Reproduced with permission from Ref. [153]. Copyright 2020, WILEY–VCH

Gan et al. [161] recently wrapped the separated 2D ultra-thin Ti_3C_2 nanosheets with 3D CF to prepare Ti_3C_2@CF sulfur matrix material, which can significantly increase their surface area. The synthetic route is shown in Fig. 5b. Because the material is a high-density uniform thin layer, it can well load sulfur on its surface, without causing any loss of electrode conductivity. There is a strong bond between Ti_3C_2 nanosheets and lithium polysulfide, which can effectively inhibit shuttle. The flexible Ti_3C_2 coating can also dramatically improve CF's ductility, which has an excellent ability to withstand the deformation and stress caused by volume expansion, thereby avoiding cathode powdering. The LSBs thus obtained has impressive cycle stability, and its capacity decay rate is negligible (at 0.5 °C, the capacity of the first 200 cycles is 0.06%). After 1000 cycles at 1 °C, the cycle capacity is still enormous (626.0 mAh·g^{-1}).

To obtain high-performance LSBs, the improvement of high-sulfur surface-loaded LSBs has aroused the attention of many researchers [162]. In order to better suppress the shuttle effect in lithium-sulfur batteries, Li et al. [163] reported the preparation of a functional separator, which was modified by loading $Ti_3C_2T_x$ nanosheet coatings of different masses on the separator to effectively block and capture soluble lipopolysaccharide intermediates. In lithium-sulfur batteries, rapid lithium-ion transmission is achieved. Recently, Zhang et al. [164] used electrostatic self-assembly methods to analyze the separator's intermediate layer and sulfur host (Fig. 5c). A Ketjen black/sulfur (KB/S)@$Ti_3C_2T_x$ with interwoven structure was synthesized, in which MXene nanosheets can chemically/physically adsorb soluble polysulfides, the KB carbon core is beneficial for the improvement of electrical conductivity. This interlaced structure is beneficial to the structural integrity during the volume expansion/contraction of the sulfur electrode. However, KB@$Ti_3C_2T_x$ is applied as an intermediate layer on the diaphragm (about 3 μm), which further prevents the possible escape of polysulfides from the cathode. In order to make the interlayer not lose the weight energy density/volume, only the intermediate layer can have the slightest weight ratio and thickness, which delays the activation of dissolved polysulfides and improves the overall utilization of sulfur. Combining the effective KB@$Ti_3C_2T_x$ modified diaphragm and KB/S@$Ti_3C_2T_x$ cathode makes it possible to obtain a

stable Li–S battery with a high sulfur surface load in a relatively poor electrolyte.

Subsequently, Zhang et al. [153] injected a monoatomic zinc layer into MXene to synthesize single-atom zinc implanted MXene (SA-Zn-MXene). This layer has a superior affinity for polysulfides and thus can significantly reduce the rate-limiting step and greatly reduce the conversion energy barrier of Li_2S_2 and Li_2S. At the same time, the redox rate of polysulfides is also increased.

As shown in Fig. 5d, the CV curve of SA-Zn-MXene has four peaks at − 0.58, 0.06, 0.63, and − 0.07 V. The first dominant peak at − 0.58 V is due to the reduction of Li_2S_6 to Li_2S_2/Li_2S on the working electrode. Simultaneously, there are two peaks at 0.06 and 0.63 V, mainly due to the reduction and oxidation between the S on the working electrode and Li_2S_6. The peak at − 0.07 V can be attributed to the oxidation of Li_2S_2/Li_2S to Li_2S_6 on the same electrode. The four peaks in CV curve of SA-Zn-MXene have higher current densities than MXene (for instance, the current density of SA-Zn-MXene is 6 times higher than that of MXene at the peak of 0.63 V), implying that the monoatomic zinc MXene can greatly improve the kinetics of these redox reactions. The constant potential nucleation analysis at 2.05 V further proved this catalytic effect.

In addition, the SA-Zn-MXene layer can help promote the nucleation of Li_2S_2/Li_2S on the surface of the SA-Zn-MXene layer exposed in a large area. Such unique characteristics endow SA-Zn-MXene with a high-rate capability of up to 6.0C and a reversible capacity ($\approx$1136 $mAh{\cdot}g^{-1}$). Some researchers have applied SA-Zn-MXene to make MXene sulfur cathode, which has a high-rate capacity (640 $mAh{\cdot}g^{-1}$ at 6.0C), high area capacity (5.3 $mAh{\cdot}cm^{-2}$) and good circulation stability. The capacity retention rate after 200 cycles at 4.0C still reaches 80% [164].

3 Supercapacitor

With the continuous growth of human society's demand for clean energy, the development of new energy storage equipment is crucial [165]. As a major kind of energy storage device, supercapacitors attracted heated attention due to their unique electrochemical properties such as superior rate performance, high power density, long cycle life, and excellent safety [44, 166–171]. Supercapacitors are generally classified into pseudo-capacitors and electric double-layer capacitors (EDLCs) based on their energy storage mechanism. First of all, in a pseudo-capacitor, the charge is stored by Faraday oxidation–reduction reaction. Secondly, EDLCs realize electrostatic charge storage by separating ions in the Helmholtz double layer on the electrode surface [144, 172–174]. When the number of active materials of EDLCs is limited, the energy density will be relatively low, which limits its application in real life. In contrast, pseudo-capacitors can provide higher energy density, however, the cycle of life is shorter [175–177].

3.1 Electric double-layer capacitor

An electric double-layer capacitor is a new type of energy storage element between batteries and traditional capacitors. It has high energy density and power density, fast charging speed, long cycle life, and no pollution to the environment. It is widely used in practical applications. MXene has great application prospects in batteries, supercapacitors, electrocatalysts and photocatalysts, and has attracted many researchers' attention. MXene electrode shows a high capacitance in an aqueous solution. Still, in a non-aqueous solution, it will show an even higher capacitance and a wider voltage window, which can further increase the energy density [178–182]. However, the universal inherent shortcomings of 2D nanomaterials will limit the future development and practical application.

Therefore, to design and synthesize 2D-2D heterostructures, Wang et al. [183] designed a 2D ordered mesoporous carbon (OMC) thin layer in the interlayer space of MXene (Fig. 6a). Using MAX to synthesize the most commonly used 2D layered MXene ($Ti_3C_2T_x$), presynthesized low molecular weight phenolic resin and amphiphilic triblock copolymer F127 (PEO-PPO-PEO) were added to the $Ti_3C_2T_x$ dispersion in ethanol. Afterward, the mixed solution was in a vacuum oven to evaporate ethanol because the well-dissolved small phenolic resin molecules and F127 unimer can easily penetrate the middle layer of $Ti_3C_2T_x$, and F127 unimers and resol molecules can be embedded in the middle layer of $Ti_3C_2T_x$. With the gradual evaporation of ethanol, F127 unimers will be induced to assemble into micelles (the core is a hydrophobic PPO block). The shell is a PEO block with –OH end groups and a hydrophilic PEO block, because the sol molecules and hydrogen bonds exist mutually. The function makes the assembly of micelle@resol more and more compact, allowing the 2D ordered micelle@resol layer to exist between the $Ti_3C_2T_x$ nanosheets, resulting in $Ti_3C_2T_x$-micelle@resol composite material. To finally form a 2D-2D heterostructure (abbreviated as $Ti_3C_2T_x$-OMC), the $Ti_3C_2T_x$-micelle@resol composite material is heat-treated in an inert atmosphere to convert micelle@resol into an OMC layer. MXene-derived carbon (MDC) composed of microporous carbon nanosheets can be obtained by etching the metal on the MXene substrate, and the Ti in $Ti_3C_2T_x$-OMC is entirely removed by chlorination to get pure carbon. The highly interconnected nanopore

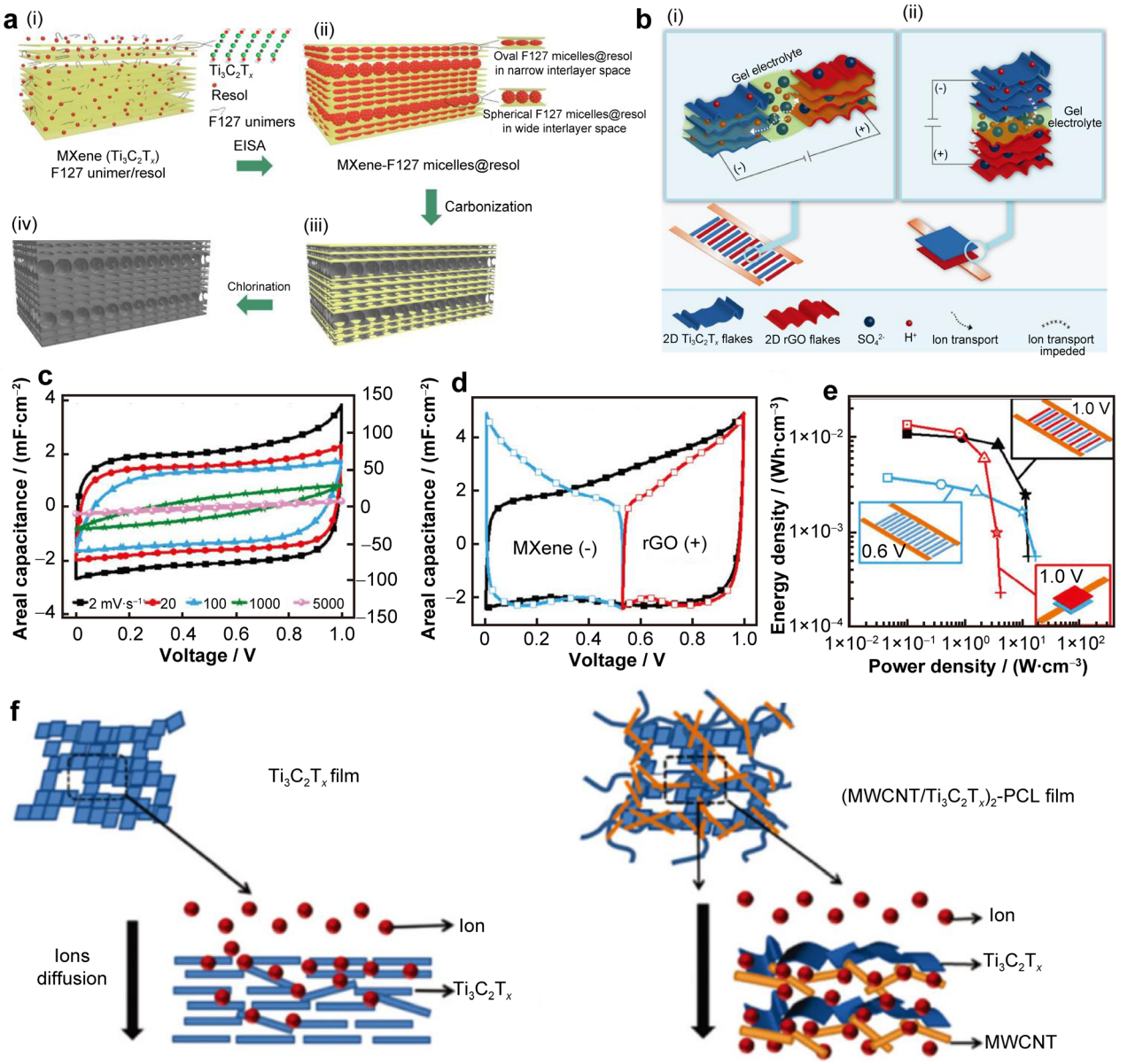

Fig. 6 **a** Schematic illustration of synthetic route: preparation of (i) MXene/F127 unimer/resol mixture, (ii) MXene-F127 micelles@resol composite, (iii) MXene-OMC composite and (iv) MDC-OMC composite. Reproduced with permission from Ref. [183]. Copyright 2017, Nature. **b** Schematic illustrations demonstrating (i) interdigitated and (ii) sandwich configurations of asymmetric MSCs, where interdigitated architecture (i) allows for facile in-plane diffusion of ions between electrodes while (ii) sandwich architecture impedes ion transport pathways between layers of the electrode materials; **c** CVcurves of asymmetric MSC at different scan rates (2–5000 mV·s^{-1}) in a 2-electrode configuration; **d** CV curves of MSC and individual electrodes recorded at 2 mV·s^{-1} in a 3-electrode configuration; **e** Ragone plots of asymmetric interdigitated MSC (black, top right), asymmetric sandwich MSC (red, bottom right), and all-MXene symmetric interdigitated MSC (blue, middle left) with scan rates ranging between 2 and 5000 mV·s^{-1}. Reproduced with permission from Ref. [184]. Copyright 2017, WILEY–VCH. **f** Schematic illustration of surface modification of PCL electro-spun fibers and schematic illustrations of ion diffusion in a $Ti_3C_2T_x$ film and a $(MWCNT/Ti_3C_2T_x)_2$-PCL film. Reproduced with permission from Ref. [185]. Copyright 2018, Royal Society of Chemistry

network between the MXene layers provides a path for ion diffusion and accelerates the electron transfer between the MXene layers. Moreover, the embedded 2D OMC prevents the re-stacking of the nanosheets.

The micro-manufacturing process of micro-supercapacitors (MSC) is relatively cumbersome, usually involves precision lithography protocols and multi-step processing. Recently, Couly et al. [184] designed and manufactured an asymmetric micro supercapacitor based on MXene, which has flexibility, no collector, and no binder. Since the device configuration and electrode structure are very important to improve the selected electrode material's electrochemical

performance, they designed two device configurations, namely, sandwich (cofacial) and interdigital (coplanar) layouts of reduced graphene oxide (rGO) and $Ti_3C_2T_x$ 2D layers, as shown in Fig. 6b. However, the difference between the two layouts is that the MXene and rGO layers face each other in the sandwich configuration. In contrast, the interdigital configuration is located on the same plane. The designed device structure uses customized masks and scalable spraying technology to fabricate interdigital shapes on flexible and transparent substrates. The electrode material is composed of rGO and titanium carbide $Ti_3C_2T_x$. Because they are both 2D layered materials, the ion diffusion rate in the interdigital electrode structure will increase significantly. In the two-electrode configuration, they tested the electrochemical performance of MSC with $Ti_3C_2T_x$-MXene as the positive electrode and rGO as the negative electrode. The CV curves of the asymmetric MSC are shown in Fig. 6c. A voltage window of 1 V and a rectangular CV shape can be observed, indicating good capacitive behavior. To distinguish the different properties of the two electrodes, a silver wire pseudo-reference was used to insert the gel electrolyte to allow the two to contact. As shown in Fig. 6d, when the symmetrical $Ti_3C_2T_x$ interdigital MSC was tested, the maximum voltage window could be 0.6 V, which illustrates the previous symmetrical configuration's narrow voltage window. It is possible to increase the total potential window to 1 V if reduced rGO was used as the positive electrode. Because of the extended voltage window, the asymmetric interdigital mesenchymal MSC will show better energy density than the symmetrical interdigital mesenchymal MSC under similar power density (Fig. 6e). The asymmetric micro supercapacitor based on MXene has an energy density of 8.6 $mWh{\cdot}cm^{-3}$ and a power density of 0.2 $W{\cdot}cm^{-3}$. It works under a voltage window with 1 V. After 10,000 cycles, it still maintains 97% of the initial value capacitance. The symmetrical devices are slightly better than asymmetrical devices at high scan rates. This may be due to that the conductivity of MXene is higher than that of rGO, which gives the full MXene symmetric device a higher rate capability, even if it exhibits a high degree of flexibility during mechanical bending.

Zhou et al. [185] developed a simple layered assembly process, mainly by spraying multi-walled carbon nanotubes (MWCNTs) and $Ti_3C_2T_x$ on the electrospun polycaprolactone (PCL) nanofiber network to form the template electrode. The MWCNTs and $Ti_3C_2T_x$ nanosheets were uniformly deposited on the PCL fiber substrate, and the obtained independent composite film was applied to the supercapacitor electrode. From the morphology of the annealed (MWCNT/$Ti_3C_2T_x$)$_2$-PCL hollow fiber, it can be seen that the MWCNTs in the multilayer composite film are helpful for the separation of $Ti_3C_2T_x$ layers. The electrolyte pathway created by combining these interlayer spacing types partially overcomes the reassembly problem of $Ti_3C_2T_x$ nanosheets. It can increase the electrolyte ion diffusion rate during the charge and discharge process and accelerate the diffusion of electrolyte ions to the electrode's inner area, as shown in Fig. 6f. The results show that the composite fiber electrode's capacitance retention rate is higher than that of the vacuum-filtered $Ti_3C_2T_x$ film at a high scan rate. When the composite film's scan rate is increased from 10 $mV{\cdot}s^{-1}$ to 100 $V{\cdot}s^{-1}$, the capacitance retention rate is 14%–16% of the initial capacitance. The standard vacuum-filtered $Ti_3C_2T_x$ thin-film electrode has a capacitance retention rate of only 1%. The easy-to-contact morphology, hierarchical structure and high porosity of these $Ti_3C_2T_x$/fiber composite membrane electrodes, as well as the inherent high capacitance of MXenes, greatly enhance their overall charge storage and high-rate performance. Besides, the composite electrode has better capacitance retention than other nanostructured electrodes. The use of 2D $Ti_3C_2T_x$ nanosheets, the synergistic effect of hierarchical nanostructures constructed by layer-by-layer (LbL) assembly, and the high accessible surface area of electrospun nanofiber scaffolds greatly improve the accessibility and diffusion of electrolyte ions in active materials. This composite membrane provides nanofiber-supported electrodes with equivalent capacitance and high flexibility, and they also maintain high conductivity and structural integrity even when they are bent or folded 100 times.

3.2 Pseudo-capacitor

Compared with battery materials for electric double-layer capacitors, pseudo-capacitor materials have a higher specific capacity and high-rate characteristics, which has prompted more and more researchers to pay attention to the research of pseudo-capacitor materials and related energy storage systems. In recent years, nanomaterials have been widely used in the field of energy storage. Among the 2D materials, MXene has attracted substantial attention in the field of EES due to its unique surface hydrophilicity, high conductivity, rich surface redox chemistry and superior mechanical properties [186–191]. The size of the carriers is a key challenge for MXene nanocomposites using multivalent water electrolytes. This requires further modification of MXene electrodes to better carry out reversible electrochemical reactions and store charges. Some researchers have found that pre-insertion of foreign species in the spacing of the MXene electrode is of great help in improving the accessibility of carriers into the electrode. So far, many nano-material interlayers, including nano-tin nanoparticles, nano-carbon and surfactants, have been inserted into the pillars of multilayer MXene electrodes

[192–198]. For example, Tian et al. [199] reported that one-dimensional (1D) cellulose nanofibers are used as functional additives to assemble MXenes. CNF has a high aspect ratio and its special interaction with MXene enables nanocomposites to have high mechanical strength without sacrificing electrochemical performance.

Conversion magnetite has attracted more and more people's attention because of its non-toxic, abundant reserves and large lithium storage capacity. However, whether it is a nanocomposite of 2D materials or original magnetite, they cannot simultaneously prevent re-stacking, crushing, and poor structural uniformity due to the lack of interfacial interaction between the layers. Recently, Wang et al. [200] synthesized and prepared 3D layered Fe_3O_4/C@MXene composites with interconnected and mesoporous/macroporous conductive networks. Figure 7a shows the synthesis process of hollow Fe_3O_4/C microspheres wrapped in several layers of MXenes (Fe_3O_4/C@MXene). MXenes after ultrasonic peeling, because of their abundant surface functional groups with inherent negative charges (i.e., hydroxyl, oxygen and fluorine functional groups), can promote dispersion in the aqueous solution. Because MXene has higher intrinsic conductivity and milder synthesis conditions (such as free of concentrated acids and strong oxidants), MXene can better replace solution-treated rGO. In addition, the Fe_3O_4 surface layer can react delicately with H^+ in the dilute inorganic acid to produce positively charged Fe(II, III) OH^{2+}. Therefore, under the condition of pH ≈ 2, the zeta potential is opposite, with a difference of 78.1 mV, which induces Fe_3O_4/PEG and MXene to form Fe_3O_4/PEG@MXene with a 3D layered open structure through electrostatic self-assembly at room temperature, and the potential of zeta is partially offset. Sequential annealing in argon can obtain Fe_3O_4/C@MXene through the constitutive electrostatic self-assembly strategy. This strategy forms an effective ion diffusion channel and an effective electron/charge transfer network by alternately arranging electroactive Fe_3O_4/C micro-spacer layers and multilayer MXene. In addition, the integration of flexible 2D MXene-coated hollow Fe_3O_4/C microspheres provides additional buffer space and constraints for the pulverization and aggregation of Fe_3O_4/C during continuous cycles. After long-term cycling, the undegraded specific capacity of 907 mAh·g^{-1} remains at 0.5 A·g^{-1}, which has good cycling stability. When used as the anode of a 4.0 V lithium-ion capacitor, a high energy density of 130 Wh·kg^{-1} can be obtained, with a maximum power density of 25,000 W·kg^{-1}.

In recent years, layered double hydroxides (LDHs) as a typical "pseudo-capacitance" electrode material have attracted researchers' attention, since LDHs exhibit typical battery-type behavior where a pair of important Faraday

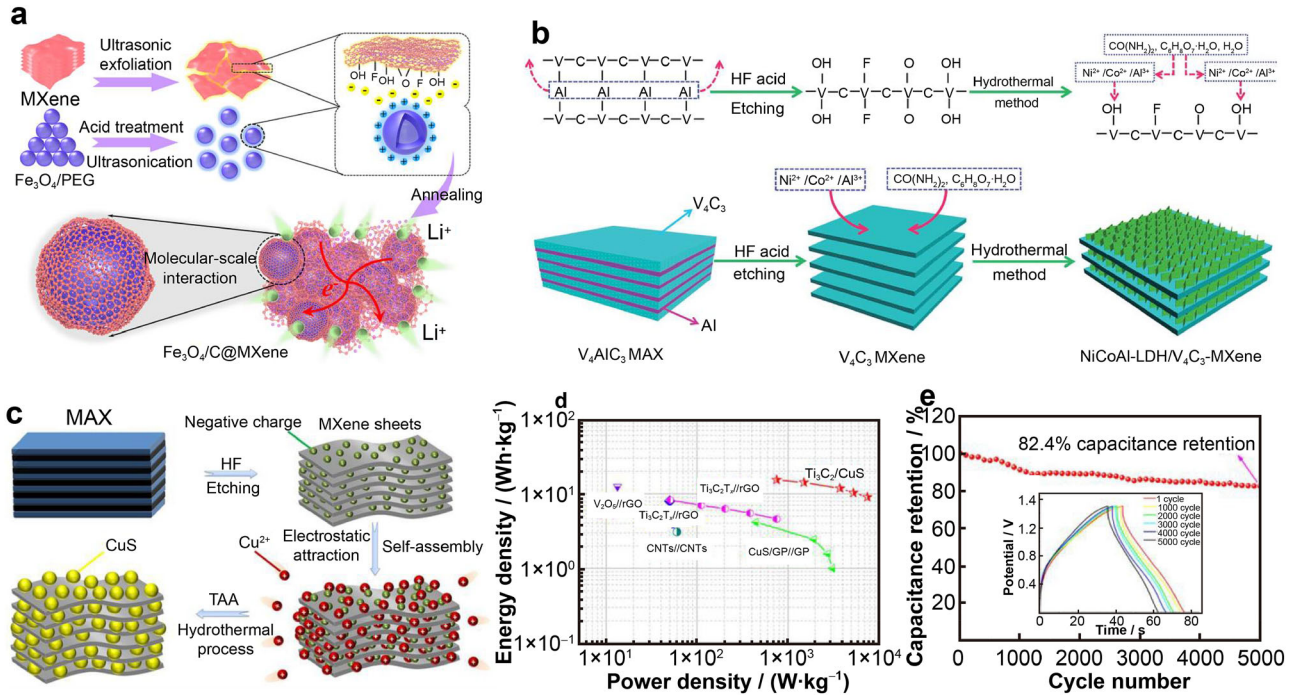

Fig. 7 **a** Thypical synthetic procedures of electrostatically self-assembled Fe_3O_4/C@MXene nanocomposites. Reproduced with permission from Ref. [200] Copyright 2020, American Chemical Society. **b** Schematic diagram of synthetic process of NiCoAl-LDH/$V_4C_3T_x$ composite; **c** scheme illustration of synthesis route of Ti_3C_2/CuS composites; **d** Ragone plots of average power density vs. energy density; **e** cycling stability at a current density of 2 A·g^{-1} over 5000 cycles. Reproduced with permission from Refs. [201, 201]. Copyright 2019, Royal Society of Chemistry

redox peaks are observed in the CV curve. They have a large potential separation, so they are considered battery-type materials. However, LDHs usually undergo irreversible phase changes during charging and discharging, which reduces their electrical conductivity and has poor rate capability. To improve its electrochemical performance, LDHs can be mixed with conductive materials. Recently, Niu et al. [201] reported the face-to-face electrostatic orderly self-assembly of monolayer MXene and edge-enriched CoAl-LDH nanosheets on the molecular scale to prepare MXene/CoAl-LDH heterostructures. Thanks to the unique structure and strong interfacial interaction between MXene and CoAl-LDH, the electrical conductivity, the accessible surface area of electrolyte ions and the number of exposed electroactive sites have increased dramatically, which can exhibit excellent electrochemical performance. Wang et al. [198] have successfully synthesized NiCoAl-LDH/$V_4C_3T_x$ heterostructures and 3D interconnected porous networks by hydrothermal methods. The microstructure of the porous network is shown in Fig. 7b. First, by etching V_4AlC_3 powder with HF, V_4C_3 MXene can be obtained. Because there are functional groups such as –OH, –O, and –F on the surface of MXene, they can be firmly fixed on the V_4C_3 MXene nanosheets, which is of great help to the nucleation of NiCoAl-LDH nanosheets. Then, the V_4C_3 MXene sheet and $C_6H_8O_7$ were dispersed in a solution containing Al^{3+}, Ni^{2+}, Co^{2+}, and urea to synthesize a 3D interconnected porous NiCoAl-LDH/$V_4C_3T_x$ composite material. In 1 mol·L^{-1} KOH, when the current density is 1 A·g^{-1}, the specific capacitance is 627 C·g^{-1}. Even at a high current density of 20 A·g^{-1}, the specific capacitance is 300 C·g^{-1}, resulting in NiCoAl-LDH/$V_4C_3T_x$ heterojunction with good rate performance. Besides, the maximum energy density of a hybrid supercapacitor composed of NiCoAl-LDH/$V_4C_3T_x$ as the battery electrode and activated carbon (AC) as the capacitor electrode in 1 mol·L^{-1} KOH is 71.7 Wh·kg^{-1}. Even with a power density of 20,000 W·kg^{-1} and a discharge time of 8.1 s, the energy density can still be maintained at 45 Wh·kg^{-1}, which shows that the NiCoAl-LDH/$V_4C_3T_x$//AC hybrid device has ultra-high-speed energy storage ability.

CuS has been used as an electrode material for supercapacitors because it has a higher theoretical capacity and chemical stability. For example, the combination of CuS nanomaterials and other 2D conductive nanostructure materials will increase the surface area, facilitate the transmission of electrons, and reduce the diffusion resistance of ions in the electrode, resulting in higher capacity. Considering the excellent chemical stability of CuS and the good electrical conductivity of Ti_3C_2 sheets, the development of Ti_3C_2/CuS composite materials as electrode materials for alkaline hybrid capacitors is of great significance to the research of electrode materials. Pan et al. [202] reported composite preparation between Cu nanoparticles and 2D Ti_3C_2, and studied their electrochemical performance. The Ti_3C_2 flakes and CuS nanoparticles were combined by the hydrothermal method. Figure 7c illustrates the preparation steps of Ti_3C_2/CuS composite material. Because the surface of Ti_3C_2 is negatively charged, positively charged Cu^{2+} are adsorbed between the layers and on the surface of Ti_3C_2, and CuS is decorated on the Ti_3C_2 sheet to form a Ti_3C_2/CuS composite material. The Ti_3C_2/CuS composite electrode in the standard three-electrode system exhibits better electrochemical performance than the Ti_3C_2 electrode and has a strong redox reaction. When the current density is 1 A·g^{-1}, the optimal specific capacity of Ti_3C_2/CuS composite electrode is as high as 169.5 C·g^{-1}, which is about five times that of Ti_3C_2. The increase in the composite electrode's specific capacity is due to the synergistic effect of the excellent electrical conductivity of Ti_3C_2 and the excellent electrochemical reaction activity of CuS. Figure 7d shows the Ragone diagram of TC-9//Ti_3C_2 ASC, which further illustrates the overall electrochemical characteristics of ASC. It can be seen that when the power density of TC-9//Ti_3C_2 is 750.2 W·kg^{-1}, the highest energy density is 15.4 Wh·kg^{-1}. TC-9//Ti_3C_2 ASC has high cycle stability at a current density of 2 A·g^{-1}, as shown in Fig. 7e, even after 5000 cycles, it still maintains 82.4% of the initial specific capacitance.

Conductive polymers have many advantages, such as good conductivity, high specific capacitance, and low cost, but they are usually prone to volume expansion and contraction during charging and discharging. Combining MXene with conductive polymers is a practical approach to obtain performance greater than each of these two. Increasing the energy of electrochemical capacitors while maintaining high power, long-term cycle stability, and safety is challenging. Ogihara et al. [203] introduced a new type of asymmetric capacitor that used an intercalated metal–organic framework (iMOF) composed of dilithium 2,6-naphthalenedicarboxylate as the negative electrode. Figure 8a shows the preparation process of the self-assembled electrode. The carboxylic acid units on the surface of 2,6-Naph $(COOLi)_2$ make it hydrophilic. In contrast, the surface of conductive nano-carbon is hydrophobic, facilitating the self-assembly of these two through hydrophilic-hydrophobic interactions. Compared with Li/Li^+, it shows a flat platform near 0.8 V, suitable for high voltage with high safety. A very thick iMOF electrode was self-assembled from conductive nano-carbon, active material, and the amphiphilic polymer was also synthesized to show higher volumetric energy density. The electrode has an efficient pathway for the transport of Li^+ and electrons. Therefore, it shows a significant area capacity

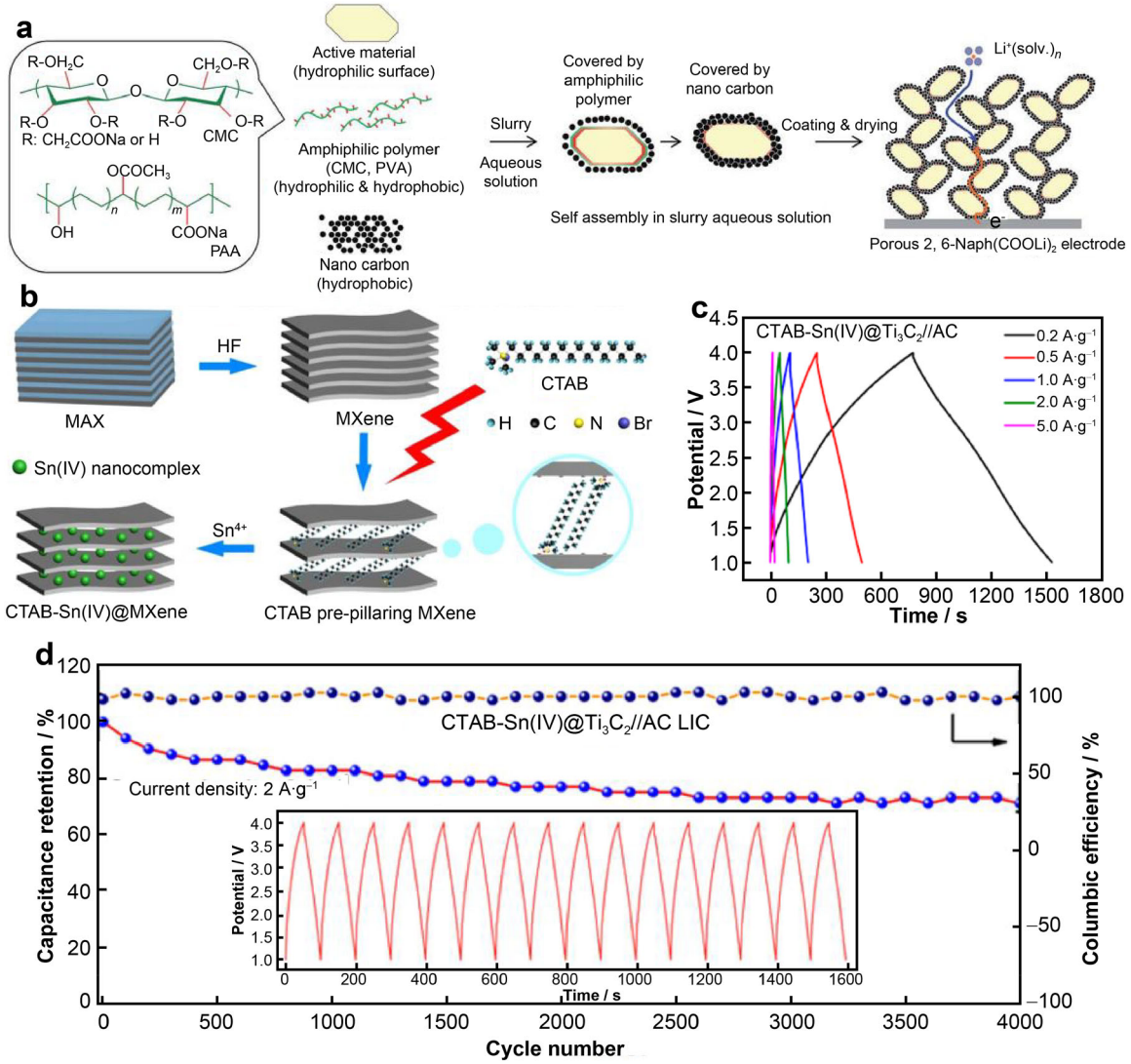

Fig. 8 **a** Schematic illustration of preparation of a porous 2,6-Naph $(COOLi)_2$ electrode from a slurry of active material and conductive nanocarbon with amphiphilic polymer. Reproduced with permission from Ref. [203]. Copyright 2016, Royal Society of Chemistry. **b** Schematic illustration of preparation of CTAB−Sn (IV)@ Ti_3C_2 by HF etching, CTAB prepillaring, and Sn^{4+} pillaring methods; **c** typical charge−discharge curves of CTAB−Sn (IV)@Ti_3C_2//AC LIC at different current densities; **d** long-term cycling performance of LIC at 2 $A{\cdot}g^{-1}$, charge−discharge curves at 2 $A{\cdot}g^{-1}$. Reproduced with permission from Ref. [204]. Copyright 2016, American Chemical Society

exceeding 2.5 $mAh{\cdot}cm^{-2}$. The asymmetric capacitor using iMOF negative electrode and activated carbon (AC) positive electrode has a high capacity (60Wh·L^{-1}) with good power and cycle stability.

To further increase the overall energy density of MXene-based LICs, how to reasonably increase and utilize the interlayer space of MXene is particularly important. Pillar-supported interlayer clay (PILCs) has attracted more attention due to its application in catalysis and separation. While maintaining the distance between the clay layers, the stabilizing pillars can also increase the layers' distance. Therefore, Luo et al. [204] tried to prepare CTAB-Sn@Ti_3C_2 from the liquid-phase cetyltrimethylammonium bromide (CTAB), Sn^{4+}, and Ti_3C_2 MXene using the pillaring method (Fig. 8b). The interlayer spacing of Ti_3C_2 can be controlled according to the intercalation agent's size (cationic surfactant). The maximum interlayer spacing can increases 177% compared to the original spacing, reaching 2.708 nm. The higher power density was obtained based on the weight and column effect of CTAB-Sn@Ti_3C_2, while the assembled LIC still has a higher energy density. When the CTAB-Sn@Ti_3C_2 anode is coupled with commercial AC cathode, the power density and energy density of LIC are higher than those of traditional MXene materials. Owing to the different energy storage mechanisms of the anode and cathode, the rectangular CV of CTAB-

Sne@Ti_3C_2//AC LIC is different from the ideal rectangular CV. When the scan rate increases, the shape of the CV remains unchanged. The charge and discharge curves are shown in Fig. 8c. These curves present almost oblique straight lines. For CTAB-Sn@Ti_3C_2//AC LIC at current densities of 0.2, 0.5, 1, 2, 5 $A{\cdot}g^{-1}$, the specific capacitance values are 51, 42, 34, 33, 25 $F{\cdot}g^{-1}$. The CTAB-Sn@Ti_3C_2// AC LIC also exhibits good cycle performance. Under the condition of 2 $A{\cdot}g^{-1}$ after 4000 cycles, the capacity retention rate is 71.1% (Fig. 8d), and the coulombic efficiency during cycling is close to 100%.

4 Catalysts

Unlike short-term energy storage strategies (such as batteries and supercapacitors), catalytic conversion of simple molecules into value-added chemicals is a longer-term solution to the world energy crisis. In the past few years, significant advances in low-cost calculations and density functional theory have made it possible to design materials from basic physical equations. The shift to a theoretically guided material design paradigm is expected to enhance the discovery and development process of catalysts by providing proper guidance to screen feasible MXene catalysts faster than experimental methods [205, 206].

4.1 Photocatalysts

Because of the abundant exposed metal sites and excellent electrical conductivity of MXenes, they can effectively transfer/separate photo-induced carriers and provide many active surface sites in catalytic reactions. Therefore, they show great promise as co-catalysts in photocatalysis. In addition, MXenes has unique photothermal conversion characteristics, which can significantly improve the activity of the catalyst and increase the reaction rate. More importantly, the unique 2D structure of MXene with abundant surface groups helps build 2D/2D heterojunctions based on MXene and 2D semiconductors. A firm interface contact can be established between the photocatalyst and the promoter. This kind of 2D/2D heterojunction with close contact, due to its strong physical properties and electronic coupling, can significantly help the separation and transfer of light-induced carriers at the heterojunction interface and can effectively improve the photocatalytic performance of nanosheets, although the aggregation of nanoplatelets may result in a smaller surface area. Compared with 0D/2D and 1D/2D composite materials, 2D/2D compact heterojunctions have a larger contact surface, ensuring better structural stability [207–210].

Recently, Cao et al. [211] successfully synthesized 2D/2D heterojunction of ultra-thin Ti_3C_2/Bi_2WO nanosheets by growing Bi_2WO_6 ultra-thin nanosheets in situ on the surface of Ti_3C_2 ultra-thin nanosheets. The synthesis process is shown in Fig. 9a. First, Ti_3AlC_2 was etched into an accordion-shaped structure using HF. Then, ultra-thin Ti_3C_2 nanosheets were prepared using the dimethyl sulfoxide (DMSO) intercalation-assisted ultrasonic peeling method, after which they were put in the $Bi(NO_3)_3$ aqueous solution. Because Ti_3C_2 nanosheets have abundant negative potential end groups (–O or –OH), they have a strong adsorption effect on Bi^{3+} cations. Then, the Na_2WO_6-CTAB mixed solution was added to the above suspension and subjected to hydrothermal treatment. The electrostatic attraction between Ti_3C_2 and Bi^{3+} cations can ensure that Bi_2WO_6 grows in situ on the surface of Ti_3C_2, resulting in intimate contact between Ti_3C_2 and Bi_2WO_6. The resultant Ti_3C_2/Bi_2WO_6 has a polyatomic layered hybrid structure and has significant photocatalytic CO_2 reduction performance. The total output of CH_4 and CH_3OH is much greater than the that of the original Bi_2WO_6 ultra-thin nanosheets because the Ti_3C_2/Bi_2WO_6 2D/2D heterojunction has a relatively short charge transport distance and a large interface contact area, which promotes the effective transfer of electrons from the photocatalyst (Bi_2WO_6) to the cocatalyst (Ti_3C_2). In addition, the improvement of the pore structure and specific surface area of the 2D/2D heterostructure ultra-thin nanosheets significantly enhanced its CO_2 adsorption capacity, thereby further promoting the photocatalytic reaction.

The guar-based polymer carbon nitride (CNs) with a special 2D layered structure has been applied in photocatalysis because it is chemically and thermally stable, and its electronic properties and optics are chemically and thermally stable. C_3N_4 has a negative reduction potential (1.2 eV) and a narrow band gap (2.8 eV). It is integrated with TiO_2 to design and synthesize an s-type heterojunction photocatalyst, a promising candidate material. Recent research has focused on synthesizing TiO_2/C_3N_4 composite materials, with greatly improved photocatalytic activity. He et al. [212] synthesized a core–shell structured TiO_2/C_3N_4 composite material. The surface of C_3N_4 was modified with telomere Ti_3C_2 quantum dots (TCQD) to effectively reduce CO_2 to hydrocarbon fuel. The interface assembly of TCQD on TiO_2/C_3N_4 core–shell nanosheets is shown in Fig. 9b. By using the amphiphilic Pluronic triblock copolymer F127 as the bridging agent and glycerol as the specific structure-directing agent, 2D TiO_2 nanosheets with single-layer mesopores were synthesized by hydrothermal-induced solvent-constrained single micelle self-assembly. 2D TiO_2 nanosheets are crystallized by calcining the nanosheets. Based on a given pretreatment, the precursor is urea. Through calcination, an ultra-thin C_3N_4 shell layer is deposited on the surface of TiO_2 to ensure that the mesoporous nanosheets can capture and anchor urea molecules. Water-soluble TCQD can be

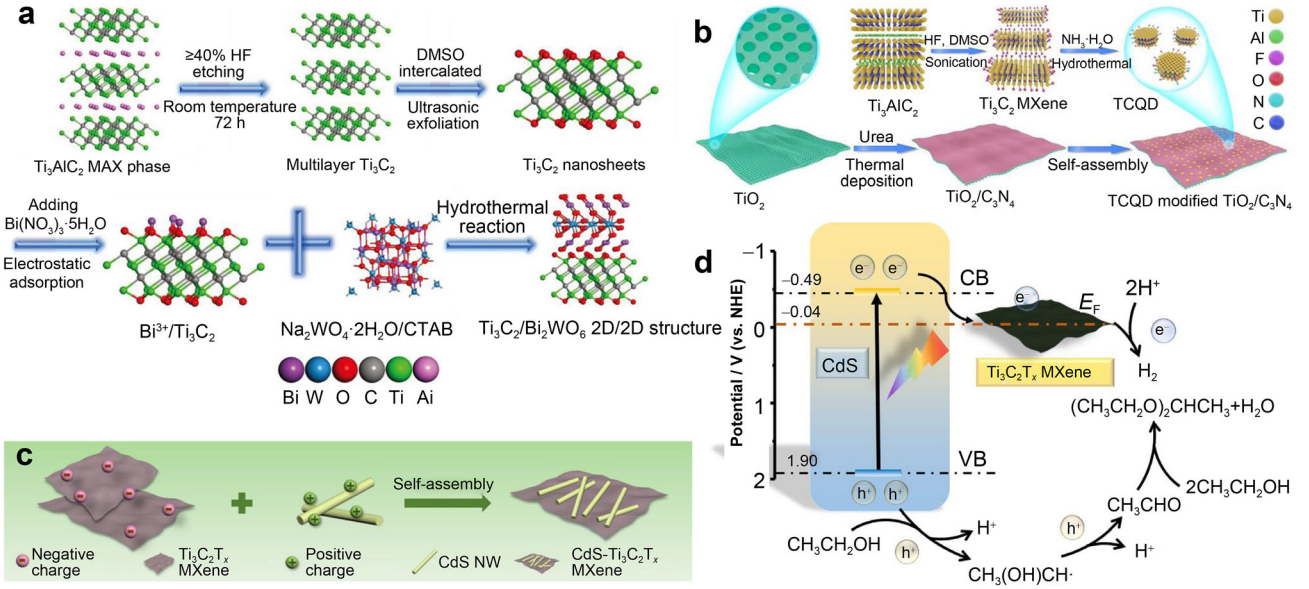

Fig. 9 **a** Schematic illustration of synthetic process of 2D/2D heterojunction of ultrathin Ti_3C_2/Bi_2WO_6 nanosheets. Reproduced with permission from Ref. [211]. Copyright 2018, Wiley–VCH. **b** Schematic illustration of synthesis of ultrathin TCQD anchored TiO_2/C_3N_4 core–shell nanosheets; **c** flowchart for preparation of binary CdS-MX heterostructures; **d** illustration of the proposed reaction mechanism for photocatalytic H_2 evolution integrated with ethanol conversion over CdS-MX composites under visible light irradiation in ethanol containing 30 mmol·L^{-1} H_2SO_4. Reproduced with permission from Refs. [212, 212]. Copyright 2020, Elsevier

obtained by a simple two-step method. First, Ti_3AlC_2 can selectively etch the Al layer by HF to synthesize layered Ti_3C_2. Then, the functionalized TCQD ending in –OH, –NH, –O, –F is passivated by the ammonia solution in the ultrasonic and surface heating method under a protective nitrogen atmosphere. During the hydrothermal treatment of amino groups, the nucleophilic substitution reaction between ammonia and epoxy groups produces secondary and primary amines. With the help of mechanical force, the well-defined TCQD is produced by the rupture of the surrounding oxygen bonds and the direct binding of the amine group to the Ti_3C_2 side at the same time. Using the enriched termination state of TCQD, TCQD was assembled on the surface of C_3N_4 through ultrasonic assistance, electrostatic action and long-term stirring, resulting in T-CN-TC composite material. The zero-distance contact between the ultra-thin core–shell nanosheets and the strong coupling between C_3N_4 and TCQD are obtained through this mechanism, which provides an effective transmission channel for carriers. It is worth noting that the s-configuration heterojunction between TiO_2 and C_3N_4 helps maintain photogenerated carriers' redox capability. The existence of TCQD accelerates the spatial migration of electrons on C_3N_4 and becomes a channel and acceptor for electron transfer. The results show that the synergy between the heterojunction and TCQD greatly enhances the photocatalytic CO_2 reduction activity. The co-degradation rate is 4.39 μmol·g^{-1}·h^{-1}, which is three times higher than that generated by C_3N_4-TiO_2 alone [212].

The comprehensive and selective conversion of bioethanol into fine chemicals and hydrogen (H_2) using solar photocatalysis is a promising approach to cope with the current energy and environmental crises, which has attracted more and more attention. Recently, Li et al. [213] reported the gentle synthesis of CdS-$Ti_3C_2T_x$ binary heterostructures (CdS-MXene) combining 1D CdS nanowires (NWs) and 2D MXene structures. An improved solvothermal method was used to prepare CdS NWs, and Ti_3AlC_2 was etched with HCl/LiF to remove the Al layer in it to prepare $Ti_3C_2T_x$ nanosheets. Figure 9c is a flow chart for electrostatic assembly of 1D CdS NW and 2D $Ti_3C_2T_x$ NSs. Bioethanol is selectively converted into 1,1-diethoxyethane (DEE) by a photocatalytic coupled redox reaction under acidic conditions. The results show that the close interface contact between the semiconducting 1D CdS NWs and the conductive 2D MXene, and the synergistic effect of matching energy level arrangement, the separation and migration of carriers have been greatly improved. Also, the photocatalytic mechanism of converting ethanol to DEE and the precipitation of H_2 by the dual-functional photocatalytic system on the CdS-MXene composite material is shown in Fig. 9d. Under visible light irradiation ($\lambda > 420$ nm), CdS NW is excited by light to generate carriers. Subsequently, due to the close contact between CdS and MXene in the CdS-MXene complex and the matching of the energy level, the photogenerated electrons tend to migrate from CdS to MXene, thereby leaving photo-induced voids on the valence band (VB) of

CdS. Therefore, ethanol is oxidized by the pores in the VB of CdS to generate the free-radical intermediate $CH(OH)CH_3$. These free radical intermediates are further oxidized to AH due to kinetic instability. Then, AH and ethanol are acetalized under acidic conditions to synthesize DEE. At the same time, the protons extracted from ethanol are reduced by photogenerated electrons to generate H_2. It is proved that $CH(OH)CH_3$ appears as a critical free-radical intermediate in the photoredox process. Facts have proved that under the premise of sustainable development, a reasonable construction of MXene-semiconductor-based composite materials will greatly promote the realization of photo-redox coupled organic synthesis and the evolution of H_2.

4.2 Electrocatalysts

MXenes has also received more and more attention from researchers in the field of electrocatalysis. As a future clean energy conversion technology, electrocatalysis is of great help in improving the future development of the field of catalysis, including hydrogen evolution reaction (HER), nitrogen reduction reaction (NRR), oxygen reduction reaction (ORR), carbon dioxide reduction reaction (CO_2RR), oxygen evolution reaction (OER) and methanol oxidation reaction (MOR). Owing to the MXene properties mentioned above, its electrocatalytic performance has become a hot research topic recently. MXenes can be used as both a catalyst and a carrier [102, 103, 214–221].

In many renewable energy storage and conversion technologies, ORR plays a key role. The platinum-based electrocatalyst is currently the most advanced ORR electrocatalyst, but the rare earth abundance is low, the stability is poor, and the price is high. There is an urgent need to develop high-performance precious metal-free ORR electrocatalysts as a substitute for platinum, but this is still a significant challenge for researchers. Therefore, Chen et al. [222] reported a strategy using a metal–organic framework (MOF) to prepare a cobalt-inlaid carbon nanotube/Ti_3C_2 nanosheet composite (Co-CNT/Ti_3C_2). The preparation process is shown in Fig. 10a. The Ti_3AlC_2 MAX phase was etched using HCl and LiF to prepare the Ti_3C_2 nano-layer. ZIF-67 particles can be grown in situ on the Ti_3C_2 nanolayer, converted into Co-CNT during the pyrolysis process. However, the Ti_3C_2 nanolayer can be used as a 2D conductive scaffold for the growth of Co-CNTs, which helps balance carbon graphitization and surface area. Because Co–N/C has abundant active sites, reasonable graphitization and suitable carbon surface area, the optimized Co-CNT/Ti_3C_2 has comparable ORR activity (half-wave potential of 0.82 V, diffusion limiting current density of 5.55 $mA{\cdot}cm^{-2}$), but has better stability than commercial Pt/C (half-wave potential is 0.82 V, diffusion limiting current density is 5.30 $mA{\cdot}cm^{-2}$), which facilitates application in renewable storage and conversion technology with unlimited possibilities.

To further improve the electrocatalytic performance, Zhao et al. [223] hybridized $Ti_3C_2T_x$ (MXene phase) nanosheets with 2D cobalt 1,4-phthalate (CoBDC) in situ through an assisted process of interdiffusion reaction. The preparation process of $Ti_3C_2T_x$ nanosheets and OER's $Ti_3C_2T_x$-MOF hybrid formation are shown in Fig. 10b. The hybrid material was applied to the OER. The hybrid material obtained a current density of 10 $mA{\cdot}cm^{-2}$ on a reversible hydrogen electrode with a potential of 1.64 V, and the Tafel slope at 0.1 $mol{\cdot}L^{-1}$ KOH was 48.2 $mV{\cdot}dec^{-1}$. These results are better than those of standard IrO_2-based catalysts and are comparable or even better than the results of the most advanced transition metal-based catalysts previously reported. Although the CoBDC layer provides a large active surface area and a highly porous structure, the $Ti_3C_2T_x$ nanosheets are conductive and hydrophilic, which can quickly transfer ions and charges on the $Ti_3C_2T_x$-CoBDC interface, and accelerate the contact of the catalytically active CoBDC surface with the water-electrolyte. The hybrid nanosheets were further made into the air cathode of a rechargeable zinc-air battery and successfully applied to light-emitting diodes' power supply. Moreover, Wen et al. [224] used a simple in-situ co-precipitation method to directly grow 2D cerium-doped NiFe layered double hydroxide nanosheets on the surface of 2D $Ti_3C_2T_x$ MXene. Owing to the synergistic effect of cerium doping and MXene coupling, the obtained NiFeCe-LDH/MXene hybrid material presents a hierarchical nanoporous structure, high electrical conductivity and strong interface bonding. Therefore, the hybrid catalyst exhibits excellent catalytic activity for OER. When the current density is 10 $mA{\cdot}cm^{-2}$ in an alkaline medium, it provides a low initial overpotential of 197 mV and an overpotential of 260 mV, which are much lower than those of its pure LDH counterpart and IrO_2 catalyst.

However, there are few reports on $Ti_3C_2T_x$ as a dual-function electrocatalyst for ORR and MOR. Some researchers have tried to develop new dual-function electrocatalysts. Because $Ti_3C_2T_x$QDs and MoS_2QDs have good catalytic activity, the ideal choice for preparing new MOR and ORR electrocatalysts is to synthesize the composite material of MoS_2QDs and $Ti_3C_2T_x$QDs with MWCNT embedded in an alkaline solution. Van der Waals force can be used on the surface of MWCNTs to modify the surface of MoS_2QD, while $Ti_3C_2T_x$ quantum dots can be fixed on the surface of COOH-functionalized MWCNTs through electrostatic interaction. Subsequently, Yang et al. [225] synthesized a new type of composite multilayer carbon nanotubes (heat-bonded) decorated with $Ti_3C_2T_x$ and molybdenum disulfide QDs (MoS_2QDs@$Ti_3C_2T_x$QDs@MWCNTs). Among them, $Ti_3C_2T_x$QDs

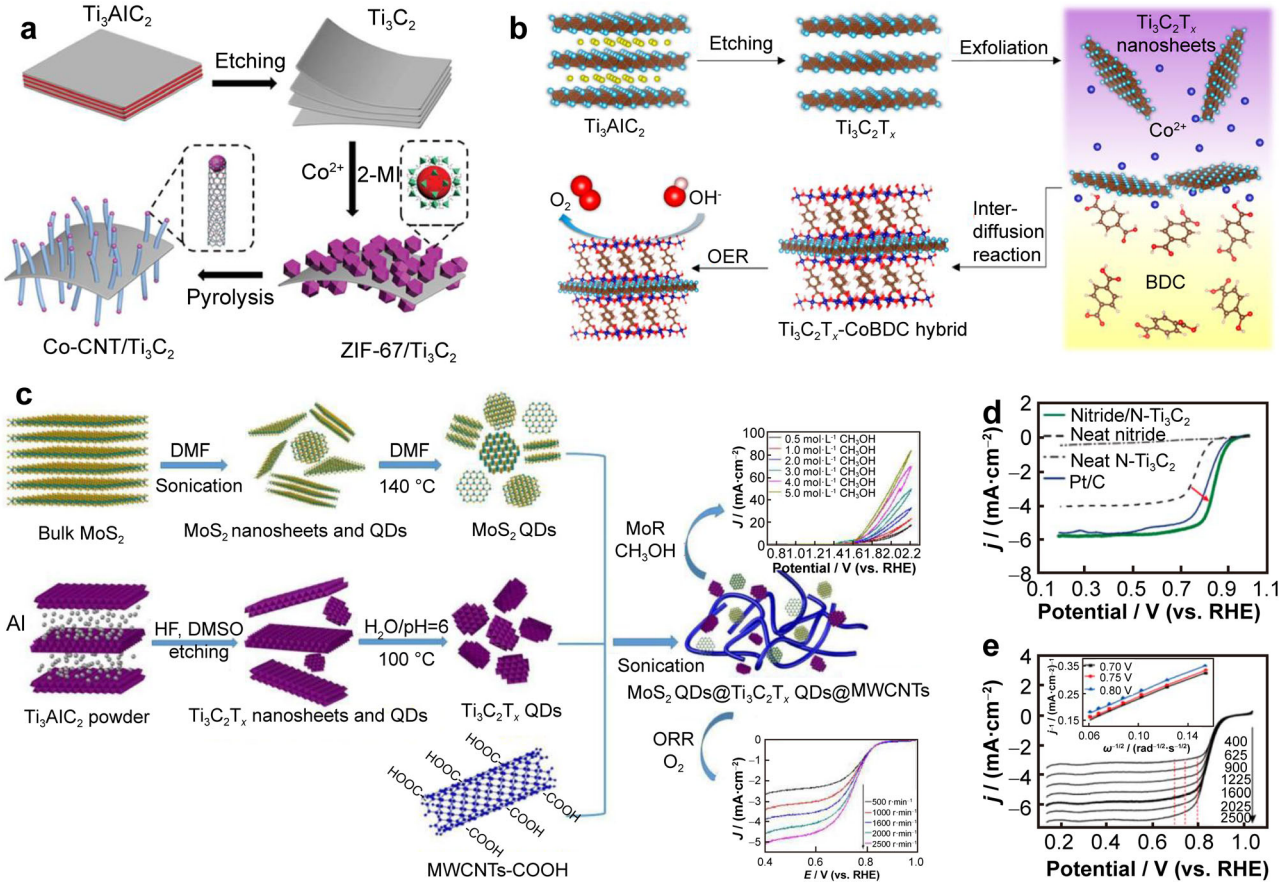

Fig. 10 **a** Schematic illustration describing formation process of CoCNT/Ti_3C_2 composites. Reproduced with permission from Ref. [220]. Copyright 2019, Royal Society of Chemistry. **b** Schematic illustration of preparation process of $Ti_3C_2T_x$ – CoBDC hybrid for OER. Reproduced with permission from Ref. [223]. Copyright 2017, American Chemical Society. **c** Schematic diagram of MoS_2QDs@$Ti_3C_2T_x$QDs@MWCNTs–2 composite preparation procedure as bifunctional catalyst for ORR and MOR in alkaline solution. Reproduced with permission from Ref. [223]. Copyright 2018, Elsevier. **d** ORR polarization curve of designed electrocatalyst compared with those of individual components and noble metals; **e** ORR polarization curves of electrocatalyst at different rotation speeds (from 400 to 2500 r·min^{-1}). Reproduced with permission from Ref. [224]. Copyright 2020, American Chemical Society

and MoS_2QDs are prepared, as exhibited in Fig. 10c. The electrochemical results show that MoS_2QDs@$Ti_3C_2T_x$QDs@MWCNTs has good catalytic activity for ORR and MOR, mainly due to the electrochemical activity, good catalytic function and specific surface area of these components. Compared with conventional electrocatalysts, the obtained MoS_2QDs@$Ti_3C_2T_x$QDs@MWCNTs embodies three advantages: low cost, feasible preparation process, and no platinum. The results show that the prepared MoS_2QDs@$Ti_3C_2T_x$QDs@MMWCNTs composite material is rich in functional groups and has good electrochemical activity. In particular, combining the excellent electrochemical performance of MoS_2QDs and $Ti_3C_2T_x$QDs with superior electrocatalytic activity, the synthesized MoS_2QDs@$Ti_3C_2T_x$QDs@MWCNTs composite materials, whether they are ORR in alkaline solution or MOR both show excellent bifunctional electrocatalytic performance. At the same time, MoS_2QDs@$Ti_3C_2T_x$QDs@MMWCNTs catalysts show better ORR activity than other non-Pt catalysts, with high half-potential ($E_{1/2}$ = 0.75 V) and low Tafel slope (90 mV·dec^{-1}), close to commercial Pt/C (20%) catalyst (Tafel slope of 89 mV·dec^{-1}, $E_{1/2}$ = 0.80 V). Besides, in alkaline solution, MoS_2QDs@$Ti_3C_2T_x$QDs@MMWCNTs also have good electro-oxidation performance for methanol. Therefore, the maximum oxidation current density of methanol at 2.2 V is 160 A·g^{-1}. The results show that the combination of MoS_2 and $Ti_3C_2T_x$QDs with MWCNT provides the potential for the preparation of ORR and MOR bifunctional electrocatalysts.

Recently, Wu et al. [226] designed and studied a detrimental nitride electrocatalyst in the form of unusual molecular flakes, and metal titanium carbide flakes stabilized the catalyst. The electrocatalytic activity of pure trimetallic nitride without Ti_3C_2 (in nano form), 20 wt% Pt

(referred to as Pt/C) supported on carbon, and pure Ti_3C_2 after the same annealing treatment were studied. The electrocatalyst designed has a higher positive charge than all other control samples (including Pt/C) when scanning the cathode peak position by CV, indicating good ORR activity. The outline of linear sweep voltammetry (LSV) is shown in Fig. 10d. The electrocatalyst showed a significantly right-shifted onset potential (0.95 V, vs. reversible hydrogen electrode) and halfwave potential ($E_{1/2}$ = 0.84 V, vs. reversible hydrogen electrode), as well as a substantially higher limiting current density (5.95 $mA{\cdot}cm^{-2}$) than Pt/C and the individual nitride. According to reports, Ti_3C_2 alone has almost no ORR reactivity. As shown in Fig. 10e, to explain the ORR kinetics, one can observe the ORR polarization curves of the catalyst at different speeds of the rotating disk electrode. According to the corresponding Koutecky-Levich diagram calculation, as the rotational speed increases linearly, the current density also increases, and the number of electrons transferred per oxygen is 3.94. The rotating disk electrode's measurement also confirmed that the number of electrons transferred is close to 4. The yield and peroxidation are even lower than 4%. This shows that the catalyst catalyzes the ORR reaction directly in the four-electron path, and in addition to the oxygen decomposition reaction. It is expected to increase the catalytic activity and release an excellent activity for catalytic ORR at half-wave potentials as low as 0.84 V. A flexible fibrous zinc-air battery was fabricated where the gel uses a designed electrocatalyst, and the electrolyte is an air cathode. It exhibits enhanced long-lasting electrochemical performance and a competitive energy density of 627 $Wh{\cdot}kg_{Zn}^{-1}$. This work has opened up a new way to apply MXene materials in future portable devices and wearable applications. Moreover, FePc and $Ti_3C_2T_x$ MXene were chosen as model catalysts and supports. Since $Ti_3C_2T_x$ MXene has surface terminals including hydroxyl and fluorine, when FeN_4 parts adhere to the $Ti_3C_2T_x$ surface by van der Waals forces, they can interact with four-coordinated Fe (II) strongly and weaken the Fe–N bond or hydrogen bond. The coupling of FePc and $Ti_3C_2T_x$ MXene leads to significant Fe 3d electron delocalization and spin configuration changes. These strong interactions make it easier for FeN_4 active sites to absorb the involved reactive species, and achieve a dual enhancement of the inherent ORR activity of FePc catalysts, thereby promoting ORR catalysis [227–229].

5 Summary and outlook

The development of advanced electrode materials plays a crucial role in developing high-performance EES and conversion devices. In the past decades, graphene research has prompted people to explore other 2D materials for such applications. One new yet up-and-coming candidate is MXene, which possesses many outstanding properties, including high melting point, hardness, high electrical and thermal conductivity, excellent antioxidant properties, hydrophilic properties, and high surface area. MXenes have presented great promise as electrode materials for energy-related applications.

However, in these applications, as with other 2D materials, MXene layers are easily stacked together to form a very dense structure, which significantly reduces the specific surface area, hinders the transport of ions, and limits the effective loading of other functional material on the surface, thereby decreasing performances. In addition, due to the inherent shortcomings of a single electrode material, electrodes or catalysts made of single-phase MXene may not meet specific practical application requirements. MXene-based composite materials with enhanced electrochemical performance based on morphology control through nano-engineering technology and surface modification are highly sought after to solve these challenges.

By designing different microstructures, such as 3D hybrid structure and sandwiched structure, ideal pore size, pore size distribution and specific surface area can be produced on the MXene-based composite to improve their comprehensive performances such as the reversible capacity and cycle life of the MXene-based electrodes in electrochemical reactions. Although there have been many researches on this front, further efforts are required to reveal the relationship between electrochemical performance and structure. This article reviews the recent research progress of MXene nanocomposites in the fields of energy storage such as batteries, supercapacitors, and catalysis. Although significant progress has been made in the past few years, some major challenges need to be resolved to promote their practical applications.

To etch the MAX phase to obtain MXene, the use of fluorine-based etchants will inevitably produce surface functional groups such as hydroxyl, fluorine, and oxygen, which has a considerable impact on the electrochemical performance of the MXene material. To effectively realize uniform and controllable functional groups on the layered MXene, it is necessary to develop new synthesis methods. During the preparation process, the re-stacking of MXene flakes will significantly limit the effective use of its surface and restrict the accessibility of electrolyte ions. The introduction of an interlayer isolation layer can effectively inhibit the re-stacking of MXene nanosheets, thereby improving the electrochemical performance. At the same time, the thickness of 2D materials is also considered to be one of the most concerning issues. Both the reaction site and the specific surface area can be significantly increased

as the thickness of the 2D material decreases. Morphology modification is thus significant, and it is also crucial to increase the active site, specific surface area and pore volume to improve performance. For future research, we believe that the following aspects are worthy of attention.

(1) Although some significant progress has been achieved on the intercalation mechanism of Li^+ and Na^+ in MXene materials via advanced in situ characterization techniques, such as in situ TEM, in situ XRD, in situ Raman spectroscopy, in situ Fourier transform infrared spectroscopy (FTIR), and in situ X-ray absorption spectroscopy (XAS), it is a critical issue to inquire deeper. The intercalation mechanism of multivalent ions, such as Al^{3+}, Mg^{2+}, or Zn^{2+}, also need to be studied. Besides, the current studies mainly focus on a few MXene materials; many other MXene materials still need to be investigated. (2) Reasonable increase and utilization of the interlayer space of MXene will further increase the specific capacitance of MXene material. The development of the pillar method may be beneficial in this area. (3) The assembly structure and chemical composition control of functional MXenes are critical to its performance. Therefore, rational design and precise manufacturing of functional MXenes will promote the application of MXenes-based high-performance devices; (4) At present, the research on MXene-based energy applications is mostly in the laboratory; to go to industrialization, the initial Coulomb efficiency of the MXene material electrode, the power density, the load density of the active material, the structural and chemical stability and of MXene during the cycle all need to be improved.

In short, the application of MXene materials in various fields has attracted more and more researches' attention and has broad development prospects. Although the energy conversion and energy storage applications of MXenes have developed rapidly in recent years, related research is still in its infancy, and there is still a long way to go before practical applications and commercial applications. We should expect more exciting and key developments in this research field shortly.

Acknowledgements This study was financially supported by the National Natural Science Foundation of China (Nos. U1904215 and 21875207), the Natural Science Foundation of Jiangsu Province (No. BK20200044), and Changjiang Scholars Program of the Ministry of Education (No. Q2018270). We also acknowledge the Priority Academic Program Development of Jiangsu Higher Education Institutions.

Declarations

Conflict of interests The authors declare that they have no conflict of interest.

References

[1] Chu S, Majumdar A. Opportunities and challenges for a sustainable energy future. Nature. 2012;488(7411):294.
[2] Lewis NS. Toward cost-effective solar energy use. Science. 2007;315(5813):798.
[3] Zhou HY, Sui ZY, Amin K, Lin LW, Wang HY, Han BH. Investigating the electrocatalysis of a Ti_3C_2/carbon hybrid in polysulfide conversion of lithium-sulfur batteries. ACS Appl Mater Interfaces. 2020;12(12):13904.
[4] Wang JT, Zhao TK, Yang ZH, Chen Y, Liu Y, Wang J, Zhai P, Wu W. MXene-based Co N-codoped porous carbon nanosheets regulating polysulfides for high-performance lithium-sulfur batteries. ACS Appl Mater Interfaces Am Chem Soc. 2019; 11(42):38654.
[5] Liang X, Garsuch A, Nazar LF. Sulfur cathodes based on conductive MXene nanosheets for high-performance lithium-sulfur batteries. Angew Chemie Int Ed. 2015;54(13): 3907.
[6] Abudakka Y, Balamurugan J, Balaji R, Kim NH, Lee JH. Advanced $Cu_{0.5}Co_{0.5}Se_2$ nanosheets and MXene electrodes for high-performance asymmetric supercapacitors. Chem Eng J. 2020;385:123455.
[7] Li S, Shi Q, Li Y, Yang J, Chang TH, Jiang J, Chen P. Intercalation of metal ions into $Ti_3C_2T_x$ MXene electrodes for high-areal-capacitance microsupercapacitors with neutral multivalent electrolytes. Adv Funct Mater. 2020;30(40): 2003721.
[8] Fan Z, Wang Y, Xie Z, Wang D, Yuan Y, Kang H, Su B, Cheng Z, Liu YY. Modified MXene/holey graphene films for advanced supercapacitor electrodes with superior energy storage. Adv Sci. 2018;5(10):1800750.
[9] Chen H, Yu L, Lin Z, Zhu Q, Zhang P, Qiao N, Xu B. Carbon nanotubes enhance flexible MXene films for high-rate supercapacitors. J Mater Sci. 2020;55(3):1148.
[10] Yu P, Cao G, Yi S, Zhang X, Li C, Sun X, Wang K, Ma Y. Binder-free 2D titanium carbide (MXene)/carbon nanotube composites for high-performance lithium-ion capacitors. Nanoscale. 2018;10(13):5906.
[11] Reddy ALM, Gowda SR, Shaijumon MM, Ajayan PM. Hybrid nanostructures for energy storage applications. Adv Mater. 2012;24(37):5045.
[12] Xie H, Geng Q, Zhu X, Luo Y, Chang L, Niu X, Shi XF, Asiri AM, Gao S, Wang Z, Sun X. PdP_2 nanoparticles-reduced graphene oxide for electrocatalytic N_2 conversion to NH_3 under ambient conditions. J Mater Chem A. 2019;7(43):24760.
[13] Handoko AD, Chen H, Lum Y, Zhang Q, Anasori B, Seh ZW. Two-dimensional titanium and molybdenum carbide MXenes as electrocatalysts for CO_2 reduction. iScience. 2020;23(6): 101181.
[14] Cui B, Hu B, Liu J, Wang M, Song Y, Tian K, Zhang Z, He L. Solution-plasma-assisted bimetallic oxide alloy nanoparticles of Pt and Pd embedded within two-dimensional $Ti_3C_2T_x$ nanosheets as highly active electrocatalysts for overall water splitting. ACS Appl Mater Interfaces. 2018;10(28):23858.
[15] Li YH, Zhang F, Chen Y, Li JY, Xu YJ. Photoredox-catalyzed biomass intermediate conversion integrated with H_2 production over $Ti_3C_2T_x$/CdS composites. Green Chem. 2020;22(1):163.
[16] Zhang X, Zhang Z, Li J, Zhao X, Wu D, Zhou Z. Ti_2CO_2 MXene: a highly active and selective photocatalyst for CO_2 reduction. J Mater Chem A. 2017;5(25):12899.
[17] Bonaccorso F, Colombo L, Yu G, Stoller M, Tozzini V, Ferrari AC, Ruoff RS, Pellegrini V. Graphene, related two-dimensional crystals, and hybrid systems for energy conversion and storage. Science. 2015;347(6217):1246501.

[18] She ZW, Kibsgaard J, Dickens CF, Chorkendorff I, Nørskov JK, Jaramillo TF. Combining theory and experiment in electrocatalysis: insights into materials design. Science. 2017;355(6321):eaad4998.
[19] Romero E, Novoderezhkin VI, Van Grondelle R. Quantum design of photosynthesis for bio-inspired solar-energy conversion. Nature. 2017;543(7645):355.
[20] Sahan N, Paksoy HO. Thermal enhancement of paraffin as a phase change material with nanomagnetite. Sol Energy Mater Sol Cells. 2014;126:56.
[21] Novoselov KS, Mishchenko A, Carvalho A, Castro Neto AH. 2D materials and van der Waals heterostructures. Science. 2016;353(6298):aac9439.
[22] Kong X, Liu Q, Zhang C, Peng Z, Chen Q. Elemental two-dimensional nanosheets beyond graphene. Chem Soc Rev. 2017;46(8):2127.
[23] Peng W, Li X. Synthesis of a sulfur-graphene composite as an enhanced metal-free photocatalyst. Nano Res. 2013;6(8):286.
[24] Yang YR, Jung JH, Kim SJ, Hamada K, Suzuki A, Kim HJ, Lee JH, Kwon OB, Lee YK, Kim J, Kim EK, Jang HJ, Kang DS, Choi JS, Lee CJ, Marshall J, Koh HY, Kim CJ, Seok H, Kim SH, Choi JH, Choi YB, Cocco L, Ryu SH, Kim JH, Suh PG. Forebrain-specific ablation of phospholipase $C\gamma_1$ causes manic-like behavior. Mol Psychiatry. 2017;22(10):1473.
[25] Zhang S, Zheng M, Lin Z, Li N, Liu Y, Zhao B, Pang H, Cao J, He P, Shi Y. Activated carbon with ultrahigh specific surface area synthesized from natural plant material for lithium-sulfur batteries. J Mater Chem A. 2014;2(38):15889.
[26] Zheng M, Qiu D, Zhao B, Ma L, Wang X, Lin Z, Pan L, Zheng Y, Shi Y. Mesoporous iron oxide directly anchored on a graphene matrix for lithium-ion battery anodes with enhanced strain accommodation. RSC Adv. 2013;3(3):699.
[27] Pan Y, Zeng W, Li L, Zhang Y, Dong Y, Ye K, Cheng K, Cao D, Wang G, Lucht BL. Surfactant assisted, one-step synthesis of Fe_3O_4 nanospheres and further modified Fe_3O_4/C with excellent lithium storage performance. J Electroanal Chem. 2018;810:248.
[28] Lei W, Liu G, Zhang J, Liu M. Black phosphorus nanostructures: recent advances in hybridization, doping and functionalization. Chem Soc Rev. 2017;46(12):3492.
[29] Shu Y, Li B, Chen J, Xu Q, Pang H, Hu X. Facile synthesis of ultrathin nickel-cobalt phosphate 2D nanosheets with enhanced electrocatalytic activity for glucose oxidation. ACS Appl Mater Interfaces. 2018;10(3):2360.
[30] Zhao Q, Zhao M, Qiu J, Lai WY, Pang H, Huang W. One dimensional silver-based nanomaterials: preparations and electrochemical applications. Small. 2017;13(38):1701091.
[31] Yu J, Mu C, Yan B, Qin X, Shen C, Xue H, Pang H. Nanoparticle/MOF composites: preparations and applications. Mater Horizons. 2017;4(4):557.
[32] Shahzad F, Alhabeb M, Hatter CB, Anasori B, Hong SM, Koo CM, Gogotsi Y. Electromagnetic interference shielding with 2D transition metal carbides (MXenes). Science. 2016;353(6304):1137.
[33] Ding L, Wei Y, Wang Y, Chen H, Caro J, Wang H. A two-dimensional lamellar membrane: MXene nanosheet stacks. Angew Chemie Int Ed. 2017;129(7):1851.
[34] Ding L, Wei Y, Li L, Zhang T, Wang H, Xue J, Ding LX, Wang S, Caro J, Gogotsi Y. MXene molecular sieving membranes for highly efficient gas separation. Nat Commun. 2018;9(1):155.
[35] Liu A, Liang X, Ren X, Guan W, Gao M, Yang Y, Yang Q, Gao L, Li Y, Ma T. Recent progress in MXene-based materials: potential high-performance electrocatalysts. Adv Funct Mater. 2020;30(38):2003437.
[36] Yin J, Zhang L, Jiao T, Zou G, Bai Z, Chen Y, Zhang Q, Xia M, Peng Q. Highly effcient catalytic performances of nitro compounds and morin via self-assembled mxene-Pd nanocomposites synthesized through self-reduction strategy. Nanomaterials. 2019;9(7):1009.
[37] Huang B, Li N, Ong WJ, Zhou N. Single atom-supported MXene: how single-atomic-site catalysts tune the high activity and selectivity of electrochemical nitrogen fixation. J Mater Chem A. 2019;7(48):27620.
[38] Li L, Wang X, Guo H, Yao G, Yu H, Tian Z, Li B, Chen L. Theoretical screening of single transition metal atoms embedded in MXene defects as superior electrocatalyst of nitrogen reduction reaction. Small Methods. 2019;3(11):1900337.
[39] Ma Y, Liu N, Li L, Hu X, Zou Z, Wang J, Luo S, Gao Y. A highly flexible and sensitive piezoresistive sensor based on MXene with greatly changed interlayer distances. Nat Commun. 2017;8(1):1207.
[40] Zhang YZ, Lee KH, Anjum DH, Sougrat R, Jiang Q, Kim H, Alshareef HN. MXenes stretch hydrogel sensor performance to new limits. Sci Adv. 2018;4(6):6547.
[41] Chen C, Xie X, Anasori B, Sarycheva A, Makaryan T, Zhao M, Urbankowski P, Miao L, Jiang J, Gogotsi Y. MoS_2-on-MXene heterostructures as highly reversible anode materials for lithium-ion batteries. Angew Chemie Int Ed. 2018;57(7):1846.
[42] Naguib M, Mashtalir O, Carle J, Presser V, Lu J, Hultman L, Gogotsi Y. Barsoum MW. Two-dimensional transition metal carbides. ACS Nano. 2012;6(2):1322.
[43] Anasori B, Lukatskaya MR, Gogotsi Y. 2D metal carbides and nitrides (MXenes) for energy storage. Nat Rev Mater. 2017;2(2):16098.
[44] Pomerantseva E, Gogotsi Y. Two-dimensional heterostructures for energy storage. Nat Energy. 2017;2(7):1.
[45] Tang X, Guo X, Wu W, Wang G. 2D Metal carbides and nitrides (MXenes) as high-performance electrode materials for lithium--based batteries. Adv Energy Mater. 2018;8(33):1801897.
[46] Zhang J, Zhao Y, Guo X, Chen C, Dong CL, Liu RS, Han CP, Li Y, Gogotsi Y, Wang G. Single platinum atoms immobilized on an MXene as an efficient catalyst for the hydrogen evolution reaction. Nat Catal. 2018;1(12):985.
[47] Carvalho A, Wang M, Zhu X, Rodin AS, Su H, Castro Neto AH. Phosphorene: from theory to applications. Nat Rev Mater. 2016;1(11):16061.
[48] Pang J, Bachmatiuk A, Yin Y, Trzebicka B, Zhao L, Fu L, Mendes RG, Gemming T, Liu Z, Rummeli MH. Applications of phosphorene and black phosphorus in energy conversion and storage devices. Adv Energy Mater. 2018;8(8):1702093.
[49] Kelly AG, Hallam T, Backes C, Harvey A, Esmaeily AS, Godwin I, Coelho J, Nicolosi V, Lauth J, Kulkarni A, Kinge S, Siebbeles LDA, Duesberg GS, Coleman JN. All-printed thin-film transistors from networks of liquid-exfoliated nanosheets. Science. 2017;356(6333):69.
[50] Gong J, Bao X. Fundamental insights into interfacial catalysis. Chem Soc Rev. 2017;46(7):1770.
[51] Qin S, Liu D, Wang G, Portehault D, Garvey CJ, Gogotsi Y, Lei W, Chen Y. High and stable ionic conductivity in 2D nanofluidic ion channels between boron nitride layers. J Am Chem Soc. 2017;139(18):6314.
[52] Zhao J, Liu H, Yu Z, Quhe R, Zhou S, Wang Y, Liu CC, Zhong H, Han N, Lu J, Yao Y, Wu K. Rise of silicene: a competitive 2D material. Prog Mater Sci. 2016;83:24.
[53] Liu J, Yang Y, Lyu P, Nachtigall P, Xu Y. Few-layer silicene nanosheets with superior lithium-storage properties. Adv Mater. 2018;30(26):1800838.
[54] Yun Q, Lu Q, Zhang X, Tan C, Zhang H. Dreidimensionale architekturen aus übergangsmetall-dichalkogenid-nanomaterialien

zur elektrochemischen energiespeicherung und -umwandlung. Angew Chemie Int Ed. 2018;130(3):634.
[55] Zhang L, Bampoulis P, Rudenko AN, Yao Q, Van Houselt A, Poelsema B, Katsnelson MI, Zandvliet HJW. Structural and electronic properties of germanene on MoS_2. Phys Rev Lett. 2016;116(25):256804.
[56] Chhowalla M, Liu Z, Zhang H. Two-dimensional transition metal dichalcogenide (TMD) nanosheets. Chem Soc Rev. 2015;44(9):2584.
[57] Guo X, Zhang G, Li Q, Xue H, Pang H. Non-noble metal-transition metal oxide materials for electrochemical energy storage. Energy Storage Mater. 2018;15:171.
[58] Naguib M, Mochalin VN, Barsoum MW, Gogotsi Y. 25th anniversary article: MXenes: a new family of two-dimensional materials. Adv Mater. 2014;26(7):992.
[59] Lei JC, Zhang X, Zhou Z. Recent advances in MXene: preparation, properties, and applications. Front Phys. 2015; 10(3):276.
[60] Yorulmaz U, Özden A, Perkgöz NK, Ay F, Sevik C. Vibrational and mechanical properties of single layer MXene structures: a first-principles investigation. Nanotechnology. 2016;27(33):335702.
[61] Jun B-M, Kim S, Heo J, Park CM, Her N, Jang M, Huang Y, Han J, Yoon Y. Review of MXenes as new nanomaterials for energy storage/delivery and selected environmental applications. Nano Res. 2019;12(3):471.
[62] Chaudhari NK, Jin H, Kim B, San Baek D, Joo SH, Lee K. MXene: an emerging two-dimensional material for future energy conversion and storage applications. J Mater Chem A. 2017;5(47):24564.
[63] Hantanasirisakul K, Gogotsi Y. Electronic and optical properties of 2D transition metal carbides and nitrides (MXenes). Adv Mater. 2018;30(52):1804779.
[64] Lai S, Jeon J, Jang SK, Xu J, Choi YJ, Park JH, Hwang E, Lee S. Surface group modification and carrier transport properties of layered transition metal carbides (Ti_2CT_x, T: –OH, –F and –O). Nanoscale. 2015;7(46):19390.
[65] Khadir S, Bon P, Vignaud D, Galopin E, McEvoy N, McCloskey D, Monneret S, Baffou G. Optical imaging and characterization of graphene and other 2D materials using quantitative phase microscopy. ACS Photonics. 2017;4(12): 3130.
[66] Halim J, Lukatskaya MR, Cook KM, Lu J, Smith CR, Näslund LÅ, May SJ, Hultman L, Gogotsi Y, Eklund P, Barsoum MW. Transparent conductive two-dimensional titanium carbide epitaxial thin films. Chem Mater. 2014;26(7):2374.
[67] Sang X, Xie Y, Lin MW, Alhabeb M, Van Aken KL, Gogotsi Y, Kent PRC, Xiao K, Unocic RR. Atomic defects in monolayer titanium carbide ($Ti_3C_2T_x$) MXene. ACS Nano. 2016; 10(10):9193.
[68] Halim J, Kota S, Lukatskaya MR, Naguib M, Zhao MQ, Moon EJ, Pitock J, Nanda J, May SJ, Gogotsi Y, Barsoum MW. Synthesis and characterization of 2D molybdenum carbide (MXene). Adv Funct Mater. 2016;26(18):3118.
[69] Mashtalir O, Lukatskaya MR, Zhao MQ, Barsoum MW, Gogotsi Y. Amine-assisted delamination of Nb_2C MXene for Li-ion energy storage devices. Adv Mater. 2015;27(23):3501.
[70] Dong Y, Chertopalov S, Maleski K, Anasori B, Hu L, Bhattacharya S, Rao AM, Gogotsi Y, Mochalin VN, Podila R. Saturable absorption in 2D Ti_3C_2 MXene thin films for passive photonic diodes. Adv Mater. 2018;30(10):1.
[71] Zhou J, Zha X, Chen FY, Ye Q, Eklund P, Du S, Huang Q. A two-dimensional zirconium carbide by selective etching of Al_3C_3 from nanolaminated $Zr_3Al_3C_5$. Angew Chemie Int Ed. 2016;55(16):5008.
[72] Alhabeb M, Maleski K, Mathis TS, Sarycheva A, Hatter CB, Uzun S, Levitt A, Gogotsi Y. Selective etching of silicon from Ti_3SiC_2 (MAX) to obtain 2D titanium carbide (MXene). Angew Chemie Int Ed. 2018;57(19):5444.
[73] Halim J, Cook KM, Naguib M, Eklund P, Gogotsi Y, Rosen J, Barsoum MW. X-ray photoelectron spectroscopy of select multi-layered transition metal carbides (MXenes). Appl Surf Sci. 2016;362:406.
[74] Naguib M, Kurtoglu M, Presser V, Lu J, Niu J, Heon M, Hultman L, Gogotsi Y, Barsoum MW. ChemInform abstract: two-dimensional nanocrystals produced by exfoliation of Ti_3AlC_2. ChemInform. 2011;42(52):201152200.
[75] Xu C, Wang L, Liu Z, Chen L, Guo J, Kang N, Ma XL, Cheng HM, Ren W. Large-area high-quality 2D ultrathin Mo_2C superconducting crystals. Nat Mater. 2015;14(11):1135.
[76] Gogotsi Y. Chemical vapour deposition: transition metal carbides go 2D. Nat Mater. 2015;14(11):1079.
[77] Zou G, Zhang Z, Guo J, Liu B, Zhang Q, Fernandez C, Peng Q. Synthesis of MXene/Ag composites for extraordinary long cycle lifetime lithium storage at high rates. ACS Appl Mater Interfaces. 2016;8(34):22280.
[78] Zhang C (John), Kim SJ, Ghidiu M, Zhao MQ, Barsoum MW, Nicolosi V, Gogotsi Y. Layered orthorhombic Nb_2O_5@$Nb_4C_3T_x$ and TiO_2@$Ti_3C_2T_x$ hierarchical composites for high performance Li-ion batteries. Adv Funct Mater. 2016; 26(23):4143
[79] Li X, Yang X, Xue H, Pang H, Xu Q. Metal–organic frameworks as a platform for clean energy applications. EnergyChem. 2020;2(2):100027.
[80] Bu F, Shakir I, Xu Y. 3D graphene composites for efficient electrochemical energy storage. Adv Mater Interfaces. 2018; 5(15):1.
[81] Yun Q, Lu Q, Zhang X, Tan C, Zhang H. Three-dimensional architectures constructed from transition-metal dichalcogenide nanomaterials for electrochemical energy storage and conversion. Angew Chemie Int Ed. 2018;57(3):626.
[82] Li J, Yuan X, Lin C, Yang Y, Xu L, Du X, Xie J, Li J, Sun J. Achieving high pseudocapacitance of 2D titanium carbide (MXene) by cation intercalation and surface modification. Adv Energy Mater. 2017; 7(15)
[83] Zhao MQ, Xie X, Ren CE, Makaryan T, Anasori B, Wang G, Gogotsi Y. Hollow MXene spheres and 3D macroporous MXene frameworks for Na-ion storage. Adv Mater. 2017; 29(37):1702410.
[84] Liu J, Bin Zhang H, Sun R, Liu Y, Liu Z, Zhou A, Yu ZZ. Hydrophobic, flexible, and lightweight MXene foams for high-performance electromagnetic-interference shielding. Adv Mater. 2017;29(38):1702367.
[85] Hong Ng VM, Huang H, Zhou K, Lee PS, Que W, Xu JZ, Kong LB. Recent progress in layered transition metal carbides and/or nitrides (MXenes) and their composites: synthesis and applications. J Mater Chem A. 2017;5(7):3039.
[86] Yang C, Tan Q, Li Q, Zhou J, Fan J, Li B, Sun J, Lv K. 2D/2D Ti_3C_2 MXene/g-C_3N_4 nanosheets heterojunction for high efficient CO_2 reduction photocatalyst: dual effects of urea. Appl Catal B Environ. 2020;268:118738.
[87] Xiao Y, Hwang JY, Sun YK. Transition metal carbide-based materials: synthesis and applications in electrochemical energy storage. J Mater Chem A. 2016;4(27):10379.
[88] Li F, Wang W, Zhao N, Xiao B, Cao P, Wu X, Ye C, Shen E, Qiu J, Zhu QH, Xie J, Zhou X, Fan L. Regulation of nicotine biosynthesis by an endogenous target mimicry of MicroRNA in Tobacco. Plant Physiol. 2015;169(2):1062.
[89] Liu C, Bai Y, Zhao Y, Yao H, Pang H. MoS_2/graphene composites: fabrication and electrochemical energy storage. Energy Storage Mater. 2020;33:470.

[90] Li X, Yin X, Xu H, Han M, Li M, Liang S, Cheng L, Zhang L. Ultralight MXene-coated, interconnected SiCnws three-dimensional lamellar foams for efficient microwave absorption in the X-band. ACS Appl Mater Interfaces. 2018;10(40):34524.
[91] Liu J, Bin ZH, Xie X, Yang R, Liu Z, Liu Y, Yu ZZ. Multifunctional, superelastic, and lightweight MXene/polyimide aerogels. Small. 2018;14(45):1802479.
[92] Liu CC, Zhzang HL, Zhi LL, Jin P, Zhao L, Li T, Zhou XM, Sun DS, Cheng GH, Sun Q, Shi L, Xia M. Correction to: CDK_5 regulates PD-L_1 expression and cell maturation in dendritic cells of CRSwNP. Inflammation. 2019;42(1):145.
[93] Aslam MK, Niu Y, Xu M. MXenes for non-lithium-ion (Na, K, Ca, Mg, and Al) batteries and supercapacitors. Adv Energy Mater. 2021;11(2):2000681.
[94] Zhao S, Nivetha R, Qiu Y, Guo X. Two-dimensional hybrid nanomaterials derived from MXenes ($Ti_3C_2T_x$) as advanced energy storage and conversion applications. Chinese Chem Lett. 2020;31(4):947.
[95] He X, Jin S, Miao L, Cai Y, Hou Y, Li H, Zhang K, Yan Z, Chen J. A 3D hydroxylated MXene/carbon nanotubes composite as a Scaffold for Dendrite-free sodium-metal electrodes. Angew Chemie Int Ed. 2020;59(38):16705.
[96] Zhang W, Zhang J, Li Y, Yang X. Facile synthesis of transition metal complexes wrapped $Ti_3C_2T_x$ by a PVP-assisted liquid impregnation strategy with enhanced electrochemical performance for supercapacitors. Ceram Int. 2020;46(10):15492.
[97] Lin J, Yu T, Han F, Yang G. Computational predictions of two-dimensional anode materials of metal-ion batteries. Wiley Interdiscip Rev Comput Mol Sci. 2020;10(5):1473.
[98] Li W, Zhang Y, Li H, Chen Z, Shang T, Wu Z, Wu Z, Zhang C, Li J, Lv W, Tao Y, Yang QH. Layered MXene protected lithium metal anode as an efficient polysulfide blocker for lithium-sulfur batteries. Batter Supercaps. 2020;3(9):892.
[99] Tao M, Zhang Y, Zhan R, Guo B, Xu Q, Xu M. A chemically bonded $CoNiO_2$ nanoparticles/MXene composite as anode for sodium-ion batteries. Mater Lett. 2018;230:173.
[100] Byeon A, Glushenkov AM, Anasori B, Urbankowski P, Li J, Byles BW, Blake B, Van Aken KL, Kota S, Pomerantseva E, Lee JW, Chen Y, Gogotsi Y. Lithium-ion capacitors with 2D Nb_2CT_x (MXene) – carbon nanotube electrodes. J Power Sources. 2016;326:686.
[101] Zhang Y, An Y, Jiang J, Dong S, Wu L, Fu R, Dou H, Zhang X. High performance aqueous sodium-ion capacitors enabled by pseudocapacitance of layered MnO_2. Energy Technol. 2018;6(11):2146.
[102] Xiao Y, Zhang W. High throughput screening of M_3C_2 MXenes for efficient CO_2 reduction conversion into hydrocarbon fuels. Nanoscale. 2020;12(14):7660.
[103] Liu N, Lu N, Yu HT, Chen S, Quan X. Efficient day-night photocatalysis performance of 2D/2D Ti_3C_2/porous g-C_3N_4 nanolayers composite and its application in the degradation of organic pollutants. Chemosphere. 2020; 246
[104] Xia W, Mahmood A, Zou R, Xu Q. Metal-organic frameworks and their derived nanostructures for electrochemical energy storage and conversion. Energy Environ Sci. 2015;8(7):1837.
[105] Cao X, Tan C, Sindoro M, Zhang H. Hybrid micro-/nano-structures derived from metal-organic frameworks: preparation and applications in energy storage and conversion. Chem Soc Rev. 2017;46(10):2660.
[106] Ni J, Li Y. Carbon nanomaterials in different dimensions for electrochemical energy storage. Adv Energy Mater. 2016;6(17):1600278.
[107] Calderon-Dominguez M, Alcalá M, Sebastián D, Zorzano A, Viana M, Serra D, Herrero L. Bioenergetics: brown adipose tissue bioenergetics: a new methodological approach. Adv Sci. 2017;4(4):2017.
[108] Liu HW, Wang LL, Meng Z, Tang X, Li YS, Xia QY, Zhao P. A clip domain serine protease involved in moulting in the silkworm, Bombyx mori: cloning, characterization, expression patterns and functional analysis. Insect Mol Biol. 2017;26(5):507.
[109] Zhang P, Soomro RA, Guan Z, Sun N, Xu B. 3D carbon-coated MXene architectures with high and ultrafast lithium/sodium-ion storage. Energy Storage Mater. 2020;29:163.
[110] Naguib M, Mashtalir O, Carle J, Presser V, Lu J, Hultman L, Gogotsi Y, Barsoum MW. Two-dimensional transition metal carbides. ACS Nano. 2012;6(2):1322.
[111] Naguib M, Kurtoglu M, Presser V, Lu J, Niu J, Heon M, Hultman L, Gogotsi Y, Barsoum MW. Two-dimensional nanocrystals produced by exfoliation of Ti_3AlC_2. Adv Mater. 2011;23(37):4248.
[112] Li S, Cao X, Schmidt CN, Xu Q, Uchaker E, Pei Y, Gao G. $TiNb_2O_7$/graphene composites as high-rate anode materials for lithium/sodium ion batteries. J Mater Chem A. 2016;4(11):4242.
[113] Naguib M, Come J, Dyatkin B, Presser V, Taberna PL, Simon P, Barsoum MW, Gogotsi Y. MXene: a promising transition metal carbide anode for lithium-ion batteries. Electrochem commun. 2012;16(1):61.
[114] Xie Y, Dall'Agnese Y, Naguib M, Gogotsi Y, Barsoum MW, Zhuang HL, Kent PRC. Prediction and characterization of MXene nanosheet anodes for non-lithium-ion batteries. ACS Nano. 2014;8(9):9606.
[115] Li S, Khurgin JB. Electroabsorption in the type II superlattices. Appl Phys Lett. 1992;60(16):1969.
[116] Palacín MR. Recent advances in rechargeable battery materials: a chemist's perspective. Chem Soc Rev. 2009;38(9):2565.
[117] Dallagnese Y, Lukatskaya MR, Cook KM, Taberna PL, Gogotsi Y, Simon P. High capacitance of surface-modified 2D titanium carbide in acidic electrolyte. Electrochem Commun. 2014;48:118.
[118] Zhang L, Li Q, Xue H, Pang H. Fabrication of Cu_2O-based Materials for lithium-ion batteries. Chemsuschem. 2018;11(10):1581.
[119] Pang J, Mendes RG, Bachmatiuk A, Zhao L, Ta HQ, Gemming T, Liu H, Liu Z, Rummeli MH. Applications of 2D MXenes in energy conversion and storage systems. Chem Soc Rev. 2019;48(1):72.
[120] Xiong D, Li X, Bai Z, Lu S. Recent advances in layered $Ti_3C_2T_x$ MXene for electrochemical energy storage. Small. 2018;14(17):1703419.
[121] Zhu S, Ge J, Liu C, Xing W. Atomic-level dispersed catalysts for PEMFCs: progress and future prospects. EnergyChem. 2019;1(3):100018.
[122] Meng J, Zhang F, Zhang L, Liu L, Chen J, Yang B, Yan X. Rolling up MXene sheets into scrolls to promote their anode performance in lithium-ion batteries. J Energy Chem. 2020;46:256.
[123] Wei C, Fei H, Tian Y, An Y, Tao Y, Li Y, Feng J. Scalable construction of SiO/wrinkled MXene composite by a simple electrostatic self-assembly strategy as anode for high-energy lithium-ion batteries. Chinese Chem Lett. 2020;31(4):980.
[124] Liu YT, Zhang P, Sun N, Anasori B, Zhu QZ, Liu H, Gogotsi Y, Xu B. Self-assembly of transition metal oxide nanostructures on MXene nanosheets for fast and stable lithium storage. Adv Mater. 2018;30(23):1707334.
[125] Mu G, Mu D, Wu B, Ma C, Bi J, Zhang L, Yang H, Wu F. Microsphere-like SiO_2/MXene hybrid material enabling high performance anode for lithium ion batteries. Small. 2020;16(3):1905430.
[126] Zhu X, Shen J, Chen X, Li Y, Peng W, Zhang G, Zhang F, Fan X. Enhanced cycling performance of Si-MXene nanohybrids as

anode for high performance lithium ion batteries. Chem Eng J. 2019;378:122212.
[127] Tang Q, Zhou Z, Shen P. Are MXenes promising anode materials for Li ion batteries computational studies on electronic properties and Li storage capability of Ti_3C_2 and $Ti_3C_2X_2$ (X = F, OH) monolayer. J Am Chem Soc. 2012; 134(40):16909.
[128] Ahmed B, Anjum DH, Gogotsi Y, Alshareef HN. Atomic layer deposition of SnO_2 on MXene for Li-ion battery anodes. Nano Energy. 2017;34:249.
[129] Ahmed B, Xia C, Alshareef HN. Electrode surface engineering by atomic layer deposition: a promising pathway toward better energy storage. Nano Today. 2016;11(2):250.
[130] Ahmed B, Shahid M, Nagaraju DH, Anjum DH, Hedhili MN, Alshareef HN. Surface passivation of MoO_3 nanorods by atomic layer deposition toward high rate durable Li ion battery anodes. ACS Appl Mater Interfaces. 2015;7(24):13154.
[131] Naguib M, Mashtalir O, Lukatskaya MR, Dyatkin B, Zhang C, Presser V, Gogotsi Y, Barsoum MW. One-step synthesis of nanocrystalline transition metal oxides on thin sheets of disordered graphitic carbon by oxidation of MXenes. Chem Commun. 2014;50(56):7420.
[132] Rakhi RB, Ahmed B, Hedhili MN, Anjum DH, Alshareef HN. Effect of postetch annealing gas composition on the structural and electrochemical properties of Ti_2CT_x MXene electrodes for supercapacitor applications. Chem Mater. 2015;27(15):5314.
[133] Zhang R, Xue Z, Qin J, Sawangphruk M, Zhang X, Liu R. NiCo-LDH/Ti_3C_2 MXene hybrid materials for lithium ion battery with high-rate capability and long cycle life. J Energy Chem. 2020;50:143.
[134] Huang X, Sun B, Chen S, Wang G. Self-assembling synthesis of free-standing nanoporous graphene-transition-metal oxide flexible electrodes for high-performance lithium-ion batteries and supercapacitors. Chem An Asian J. 2014;9(1):206.
[135] Li L, Zhou G, Shan XY, Pei S, Li F, Cheng HM. Co_3O_4 mesoporous nanostructures@graphene membrane as an integrated anode for long-life lithium-ion batteries. J Power Sources. 2014;255:52.
[136] Chen YM, Yu L, Lou XWD. Hierarchical tubular structures composed of Co_3O_4 hollow nanoparticles and carbon nanotubes for lithium storage. Angew Chemie Int Ed. 2016; 128(20):6094.
[137] Zhao M-Q, Torelli M, Ren CE, Ghidiu M, Ling Z, Anasori B, Barsoum MW, Gogotsi Y. 2D titanium carbide and transition metal oxides hybrid electrodes for Li-ion storage. Nano Energy. 2016;30:603.
[138] Fang Y, Zhang Y, Miao C, Zhu K, Chen Y, Du F, Yin J, Ye K, Cheng K, Yan J, Wang G, Cao D. MXene-derived defect-rich TiO_2@rGO as high-rate anodes for full Na ion batteries and capacitors. Nano-Micro Lett. 2020;12(1):128.
[139] Lei YJ, Yan ZC, Lai WH, Chou SL, Wang YX, Liu HK, Dou SX. Tailoring MXene-based materials for sodium-ion storage: synthesis, mechanisms, and applications. Electrochem Energy Rev. 2020;3(4):766.
[140] Shao L, Duan X, Li Y, Yuan Q, Ye H, Ding P. A new metallic In_3O_4 sheet as an anode material for sodium-ion batteries. J Phys Chem C. 2019;123(50):30213.
[141] Lv X, Song J, Lai Y, Fang J, Li J, Zhang Z. Ultrafine nanoparticles assembled Mo_2C nanoplates as promising anode materials for sodium ion batteries with excellent performance. J Energy Storage. 2016;8:205.
[142] Zhao M-Q, Ren CE, Ling Z, Lukatskaya MR, Zhang C, Van Aken KL, Barsoum MW, Gogotsi Y. Flexible MXene/carbon nanotube composite paper with high volumetric capacitance. Adv Mater. 2015;27(2):339.
[143] Dall'Agnese Y, Rozier P, Taberna PL, Gogotsi Y, Simon P. Capacitance of two-dimensional titanium carbide (MXene) and MXene/carbon nanotube composites in organic electrolytes. J Power Sources. 2016;306:510.
[144] Maughan PA, Seymour VR, Bernardo-Gavito R, Kelly DJ, Shao S, Tantisriyanurak S, Dawson R, Haigh SJ, Young RJ, Tapia-Ruiz N, Bimbo N. Porous silica-pillared MXenes with controllable interlayer distances for long-life Na-ion batteries. Langmuir. 2020;36(16):4370.
[145] Ghidiu M, Lukatskaya MR, Zhao MQ, Gogotsi Y, Barsoum MW. Conductive two-dimensional titanium carbide "clay" with high volumetric capacitance. Nature. 2015;516(7529):78.
[146] Chen C, Boota M, Xie X, Zhao M, Anasori B, Ren CE, Miao L, Jiang J, Gogotsi Y. Charge transfer induced polymerization of EDOT confined between 2D titanium carbide layers. J Mater Chem A. 2017;5(11):5260.
[147] Wang X, Wang J, Qin J, Xie X, Yang R, Cao M. Surface charge engineering for covalently assembling three-dimensional MXene network for all-climate sodium ion batteries. ACS Appl Mater Interfaces. 2020;12(35):39181.
[148] Wang N, Xu X, Liao T, Du Y, Bai Z, Dou S. Boosting sodium storage of double-shell sodium titanate microspheres constructed from 2D ultrathin nanosheets via sulfur doping. Adv Mater. 2018;30(49):1804157.
[149] Fan L, Li X. Recent advances in effective protection of sodium metal anode. Nano Energy. 2018;53:630.
[150] Tao M, Du G, Zhang Y, Gao W, Liu D, Luo Y, Jiang J, Bao S, Xu M. TiO_xN_y nanoparticles/C composites derived from MXene as anode material for potassium-ion batteries. Chem Eng J. 2019;369:828.
[151] Zhong W, Tao M, Tang W, Gao W, Yang T, Zhang Y, Zhan R, Bao SJ, Xu M. MXene-derivative pompon-like $Na_2Ti_3O_7$@C anode material for advanced sodium ion batteries. Chem Eng J. 2019;378:122209.
[152] Fang Q, Fang M, Liu X, Yu P, Ren JC, Li S, Liu W. An asymmetric Ti_2CO/WS_2heterostructure as a promising anchoring material for lithium-sulfur batteries. J Mater Chem A. 2020;8(27):13770.
[153] Zhang D, Wang S, Hu R, Gu J, Cui Y, Li B, Chen W, Liu C, Shang J, Yang S. Catalytic conversion of polysulfides on single atom zinc implanted MXene toward high-rate lithium-sulfur batteries. Adv Funct Mater. 2020;30(30):1.
[154] Wang J, Zhang Z, Yan X, Zhang S, Wu Z, Zhuang Z, Han WQ. Rational design of porous N-Ti_3C_2 MXene@CNT microspheres for high cycling stability in Li–S battery. Nano-Micro Lett. 2020; 12(1):4.
[155] Jiang Y, Deng Y, Zhang B, Hua W, Wang X, Qi Q, Lin Q, Lv W. An interlayer composed of a porous carbon sheet embedded with TiO_2 nanoparticles for stable and high rate lithium-sulfur batteries. Nanoscale. 2020;12(23):12308.
[156] Lee DK, Chae Y, Yun H, Ahn CW, Lee JW. CO_2-oxidized $Ti_3C_2T_x$-MXenes components for lithium-sulfur batteries: suppressing the shuttle phenomenon through physical and chemical adsorption. ACS Nano. 2020;14(8):9744.
[157] Wang Z, Zhang N, Yu M, Liu J, Wang S, Qiu J. Boosting redox activity on MXene-induced multifunctional collaborative interface in high Li_2S loading cathode for high-energy Li-S and metallic Li-free rechargeable batteries. J Energy Chem. 2019;37:183.
[158] Jiao L, Zhang C, Geng C, Wu S, Li H, Lv W, Tao Y, Chen Z, Zhou G, Li J, Ling G, Wang Y, Yang QH. Capture and catalytic conversion of polysulfides by in situ built TiO_2 -MXene heterostructures for lithium-sulfur batteries. Adv Energy Mater. 2019;9(19):1900219.
[159] Alhabeb M, Maleski K, Anasori B, Lelyukh P, Clark L, Sin S, Gogotsi Y. Guidelines for synthesis and processing of

two-dimensional titanium carbide ($Ti_3C_2T_x$ MXene). Chem Mater. 2017;29(18):7633.
[160] Huang X, Tang J, Luo B, Knibbe R, Lin T, Hu H, Rana M, Hu Y, Zhu X, Gu Q, Wang D, Wang L. Sandwich-like ultrathin TiS_2 nanosheets confined within N, S codoped porous carbon as an effective polysulfide promoter in lithium-sulfur batteries. Adv Energy Mater. 2019;9(32):1901872.
[161] Gan R, Yang N, Dong Q, Fu N, Wu R, Li C, Liao Q, Li J, Wei Z. Enveloping ultrathin Ti_3C_2 nanosheets on carbon fibers: a high-density sulfur loaded lithium-sulfur battery cathode with remarkable cycling stability. J Mater Chem A. 2020;8(15): 7253.
[162] Xiong C, Zhu GY, Jiang HR, Chen Q, Zhao TS. Achieving multiplexed functionality in a hierarchical MXene-based sulfur host for high-rate, high-loading lithium-sulfur batteries. Energy Storage Mater. 2020;33:147.
[163] Li N, Xie Y, Peng S, Xiong X, Han K. Ultra-lightweight $Ti_3C_2T_x$ MXene modified separator for Li–S batteries: thickness regulation enabled polysulfide inhibition and lithium ion transportation. J Energy Chem. 2020;42:116.
[164] Zhang S, Zhong N, Zhou X, Zhang M, Huang X, Yang X, Meng R, Liang X. Comprehensive design of the high-sulfur-loading Li–S battery based on MXene nanosheets. Nano-Micro Lett. 2020;12(1):112.
[165] Wan C, Jiao Y, Liang D, Wu Y, Li J. A geologic architecture system-inspired micro-/nano-heterostructure design for high-performance energy storage. Adv Energy Mater. 2018; 8(33):1802388.
[166] Yu Z, Tetard L, Zhai L, Thomas J. Supercapacitor electrode materials: nanostructures from 0 to 3 dimensions. Energy Environ Sci. 2015;8(3):702.
[167] Lin SY, Zhang X. Two-dimensional titanium carbide electrode with large mass loading for supercapacitor. J Power Sources. 2015;294:354.
[168] Wang Y, Dou H, Wang J, Ding B, Xu Y, Chang Z, Hao X. Three-dimensional porous MXene/layered double hydroxide composite for high performance supercapacitors. J Power Sources. 2016;327:221.
[169] Yan P, Zhang R, Jia J, Wu C, Zhou A, Xu J, Zhang X. Enhanced supercapacitive performance of delaminated two-dimensional titanium carbide/carbon nanotube composites in alkaline electrolyte. J Power Sources. 2015;284:38.
[170] Zhang X, Zhang Z, Zhou Z. MXene-based materials for electrochemical energy storage. J Energy Chem. 2018;27:73.
[171] Liu C, Bai Y, Wang J, Qiu Z, Pang H. Controllable synthesis of ultrathin layered transition metallic hydroxide/zeolitic imidazolate framework-67 hybrid nanosheets for high-performance supercapacitors. J Mater Chem A. 2021;9:11201.
[172] Huang W, Zhang A, Li X, Tian J, Yue L, Cui L, Zheng R, Wei D, Liu J. Multilayer NiMn layered double hydroxide nanosheets covered porous Co_3O_4 nanowire arrays with hierarchical structure for high-performance supercapacitors. J Power Sources. 2019;440:227123.
[173] Boota M, Pasini M, Galeotti F, Porzio W, Zhao MQ, Halim J, Gogotsi Y. Interaction of polar and nonpolar polyfluorenes with layers of two-dimensional titanium carbide (MXene): intercalation and pseudocapacitance. Chem Mater. 2017;29: 2731.
[174] Stenroos S, Pino-Bodas R, Ahti T. Corrigendum to: phylogeny of the family cladoniaceae (lecanoromycetes, ascomycota) based on sequences of multiple loci. Cladistics. 2019;35(5): 603.
[175] Zhang A, Zheng W, Yuan Z, Tian J, Yue L, Zheng R, Wei D, Liu J. Hierarchical NiMn-layered double hydroxides@CuO core-shell heterostructure in-situ generated on $Cu(OH)_2$ nanorod arrays for high performance supercapacitors. Chem Eng J. 2020;380:122486.
[176] Yan Y, Li B, Guo W, Pang H, Xue H. Vanadium based materials as electrode materials for high performance supercapacitors. J Power Sources. 2016;329:148.
[177] Wang Y, Xiao X, Xue H, Pang H. Zinc oxide based composite materials for advanced supercapacitors. ChemistrySelect. 2018; 3(2):550.
[178] Shao L, Xu J, Ma J, Zhai B, Li Y, Xu R, Ma Z, Zhang G, Wang C, Qiu J. MXene/RGO composite aerogels with light and high-strength for supercapacitor electrode materials. Compos Commun. 2020;19:108.
[179] Yang L, Zheng W, Zhang P, Chen J, Zhang W, Tian WB, Sun ZM. Freestanding nitrogen-doped d-Ti_3C_2 /reduced graphene oxide hybrid films for high performance supercapacitors. Electrochim Acta. 2019;300:349.
[180] Radha N, Kanakaraj A, Manohar HM, Nidhi MR, Mondal D, Nataraj SK, Ghosh D. Binder free self-standing high performance supercapacitive electrode based on graphene/titanium carbide composite aerogel. Appl Surf Sci. 2019;481:892.
[181] Wang S, Ma Z, Lv QF, Yang H. Two-dimensional $Ti_3C_2T_x$/polyaniline nanocomposite from the decoration of small-sized graphene nanosheets: promoted pseudocapacitive electrode performance for supercapacitors. ChemElectroChem. 2019;6(10):2748.
[182] Wang Z, Chen Y, Yao M, Dong J, Zhang Q, Zhang L, Zhao X. Facile fabrication of flexible rGO/MXene hybrid fiber-like electrode with high volumetric capacitance. J Power Sources. 2020;448:227398.
[183] Wang J, Tang J, Ding B, Malgras V, Chang Z, Hao X, Wang Y, Dou H, Zhang X, Yamauchi Y. Hierarchical porous carbons with layer-by-layer motif architectures from confined soft-template self-assembly in layered materials. Nat Commun. 2017;8(1):15717.
[184] Couly C, Alhabeb M, Van Aken KL, Kurra N, Gomes L, Navarro-Suárez AM, Anasori B, Alshareef HN, Gogotsi Y. Asymmetric flexible MXene-reduced graphene oxide micro-supercapacitor. Adv Electron Mater. 2018;4(1):1700339.
[185] Zhou Z, Panatdasirisuk W, Mathis TS, Anasori B, Lu C, Zhang X, Liao Z, Gogotsi Y, Yang S. Layer-by-layer assembly of MXene and carbon nanotubes on electrospun polymer films for flexible energy storage. Nanoscale. 2018;10(13):6005.
[186] Wu G, Li T, Wang Z, Li M, Wang B, Dong A. Molecular ligand-mediated assembly of multicomponent nanosheet superlattices for compact capacitive energy storage. Angew Chemie Int Ed. 2020;59(46):20628.
[187] Shi H, Zhang P, Liu Z, Park SW, Lohe MR, Wu Y, Shaygan Nia A, Yang S, Feng X. Ambient-stable two-dimensional titanium carbide (MXene) enabled by iodine etching. Angew Chemie Int Ed. 2021;60(16):8689.
[188] Tang J, Yi W, Zhong X, Zhang C (John), Xiao X, Pan F, Xu B. Laser writing of the restacked titanium carbide MXene for high performance supercapacitors. Energy Storage Mater. 2020; 32: 418.
[189] Zhu K, Jin Y, Du F, Gao S, Gao Z, Meng X, Chen G, Wei Y, Gao Y. Synthesis of Ti_2CT_x MXene as electrode materials for symmetric supercapacitor with capable volumetric capacitance. J Energy Chem. 2019;31:11.
[190] Chen N, Huang H, Xu Z, Xie Y, Xiong D, Chu X, Gu B, Zheng B, Deng W, Zhang H, Yang W. From high-yield Ti_3AlCN ceramics to high-quality Ti_3CNT_x MXenes through eliminating Al segregation. Chinese Chem Lett. 2020;31(4):1044.
[191] Wu CW, Unnikrishnan B, Chen IWP, Harroun SG, Chang HT, Huang CC. Excellent oxidation resistive MXene aqueous ink for micro-supercapacitor application. Energy Storage Mater. 2020;25:563.

[192] Zhang X, Liu Y, Dong S, Ye Z, Wei Y. Low-temperature synthesized nanocomposites with amorphous FeOOH on $Ti_3C_2T_x$ for supercapacitors. J Alloys Compd. 2018;744:507.
[193] Oyedotun KO, Momodu DY, Naguib M, Mirghni AA, Masikhwa TM, Khaleed AA, Kebede N. Electrochemical performance of two-dimensional Ti_3C_2-Mn_3O_4 nanocomposites and carbonized iron cations for hybrid supercapacitor electrodes. Electrochim Acta. 2019;301:487.
[194] Zhao J, Liu F, Li W. Phosphate ion-modified RuO_2/Ti_3C_2 composite as a high-performance supercapacitor material. Nanomaterials. 2019;9:377.
[195] Zheng W, Zhang P, Tian W, Wang Y, Zhang Y, Chen J, Sun ZM. Microwave-assisted synthesis of SnO_2-Ti_3C_2 nanocomposite for enhanced supercapacitive performance. Mater Lett. 2017;209:122.
[196] Jiang H, Wang Z, Yang Q, Hanif M, Wang Z, Dong L, Dong M. A novel $MnO_2/Ti_3C_2T_x$ MXene nanocomposite as high performance electrode materials for flexible supercapacitors. Electrochim Acta. 2018;290:695.
[197] Zhang X, Miao J, Zhang P, Zhu Q, Jiang M, Xu B. 3D crumbled MXene for high-performance supercapacitors. Chinese Chem Lett. 2020;31(9):2305.
[198] Wang X, Li H, Li H, Lin S, Bai J, Dai J, Liang C, Zhu X, Sun Y, Dou S. Heterostructures of Ni–Co–Al layered double hydroxide assembled on V_4C_3 MXene for high-energy hybrid supercapacitors. J Mater Chem A. 2019;7:2291.
[199] Tian W, Vahid Mohammadi A, Reid MS, Wang Z, Ouyang L, Erlandsson J, Pettersson T, Wågberg L, Beidaghi M, Hamedi MM. Multifunctional nanocomposites with high strength and capacitance using 2D MXene and 1D nanocellulose. Adv Mater. 2019;31(41):1902977.
[200] Wang S, Jin D, Bian Y, Wang R, Zhang L. Electrostatically fabricated three-dimensional magnetite and MXene hierarchical architecture for advanced lithium-ion capacitors. ACS Appl Mater Interfaces. 2020;12(8):9226.
[201] Niu H, Yang X, Wang Q, Jing X, Cheng K, Zhu K, Ye K, Wang G, Cao D, Yan J. Electrostatic self-assembly of MXene and edge-rich CoAl layered double hydroxide on molecular-scale with superhigh volumetric performances. J Energy Chem. 2020;46:105.
[202] Pan Z, Cao F, Hu X, Ji X. A facile method for synthesizing CuS decorated Ti_3C_2 MXene with enhanced performance for asymmetric supercapacitors. J Mater Chem A. 2019;7:8984.
[203] Ogihara N, Ozawa Y, Hiruta O. A self-assembled intercalated metal–organic framework electrode with outstanding area capacity for high volumetric energy asymmetric capacitors. J Mater Chem A. 2016;4(9):3398.
[204] Luo J, Zhang W, Yuan H, Jin C, Zhang L, Huang H, Liang C, Xia Y, Zhang J, Gan Y, Tao X. Pillared structure design of MXene with ultralarge interlayer spacing for high-performance lithium-ion capacitors. ACS Nano. 2017;11:2459.
[205] Gao G, O'Mullane AP, Du A. 2D MXenes: a new family of promising catalysts for the hydrogen evolution reaction. ACS Catal. 2017;7(1):494.
[206] Ling C, Shi L, Ouyang Y, Wang J. Searching for highly active catalysts for hydrogen evolution reaction based on O-Terminated MXenes through a simple descriptor. Chem Mater. 2016;28(24):9026.
[207] Zhong Y, Xia X, Shi F, Zhan J, Tu J, Fan HJ. Transition metal carbides and nitrides in energy storage and conversion. Adv Sci. 2017;4(3):1500286.
[208] Guo Z, Zhou J, Zhu L, Sun Z. MXene: a promising photocatalyst for water splitting. J Mater Chem A. 2016;4(29):11446.
[209] Xiao Y, Hao Z. Comment on "zero-thermal-quenching and photoluminescence tuning with assistance of carriers from defect cluster traps" by Chen et al., J. Mater. Chem. C, 2018, 6, 10687–10692. J Mater Chem C. 2020; 8(3):1151.
[210] Wang Q, Liu D, He X. Metal-organic framework-derived Fe-N-C nanohybrids as highly-efficient oxygen reduction catalysts. Wuli Huaxue Xuebao/Acta Phys Chim Sin. 2019;35(7):740.
[211] Cao S, Shen B, Tong T, Fu J, Yu J. 2D/2D heterojunction of ultrathin MXene/Bi_2WO_6 nanosheets for improved photocatalytic CO_2 reduction. Adv Funct Mater. 2018;28(21):1800136.
[212] He F, Zhu B, Cheng B, Yu J, Ho W, Macyk W. 2D/2D/0D $TiO_2/C_3N_4/Ti_3C_2$ MXene composite S-scheme photocatalyst with enhanced CO_2 reduction activity. Appl Catal B Environ. 2020;272:119006.
[213] Li JY, Li YH, Zhang F, Tang ZR, Xu YJ. Visible-light-driven integrated organic synthesis and hydrogen evolution over 1D/2D CdS-$Ti_3C_2T_x$ MXene composites. Appl Catal B Environ. 2020;269:118783.
[214] Chen Z, Fan X, Shen Z, Ruan X, Wang L, Zeng H, Wang J, An Y, Hu Y. Cu Anchored Ti_2NO_2 as high performance electrocatalyst for oxygen evolution reaction: a density functional theory study. ChemCatChem. 2020;12(16):4059.
[215] Low J, Zhang L, Tong T, Shen B, Yu J. TiO_2/MXene Ti_3C_2 composite with excellent photocatalytic CO_2 reduction activity. J Catal. 2018;361:255.
[216] Wang H, Sun Y, Wu Y, Tu W, Wu S, Yuan X, Zeng G, Xu Z, Li S, Chew JW. Electrical promotion of spatially photoinduced charge separation via interfacial-built-in quasi-alloying effect in hierarchical $Zn_2In_2S_5/Ti_3C_2(O, OH)_x$ hybrids toward efficient photocatalytic hydrogen evolution and environmental remediation. Appl Catal B Environ. 2019;245:290.
[217] Huang JJ, Liu XQ, Meng FF, He LQ, Wang JX, Wu JC, Lu XH, Tong YX, Fang PP. A facile method to produce $MoSe_2$/MXene hybrid nanoflowers with enhanced electrocatalytic activity for hydrogen evolution. J Electroanal Chem. 2020;856:113727.
[218] Li L, Huang Y, Li Y. Carbonaceous materials for electrochemical CO_2 reduction. EnergyChem. 2020;2(1):100024.
[219] Zhang Y, Zhang X, Cheng C, Yang Z. Recent progress of MXenes as the support of catalysts for the CO oxidation and oxygen reduction reaction. Chinese Chem Lett. 2020;31(4):931.
[220] Zhu JY, Liang F, Yao YC, Ma WH, Yang B. Preparation and application of metal organic frameworks derivatives in electro-catalysis. Chinese J Rare Metals. 2019;43(2):186.
[221] Wang ZY, Jiang SD, Duan CQ, Wang D, Luo SH, Liu YG. In situ synthesis of Co_3O_4 nanoparticles confined in 3D nitrogen-doped porous carbon as an efficient bifunctional oxygen electrocatalyst. Rare Met. 2020;39(12):1383.
[222] Chen J, Yuan X, Lyu F, Zhong Q, Hu H, Pan Q, Zhang Q. Integrating MXene nanosheets with cobalt-tipped carbon nanotubes for an efficient oxygen reduction reaction. J Mater Chem A. 2019;7(3):1281.
[223] Zhao L, Dong B, Li S, Zhou L, Lai L, Wang Z, Zhao S, Han M, Gao K, Lu M, Xie X, Chen B, Liu Z, Wang X, Zhang H, Li H, Liu J, Zhang H, Huang X, Huang W. Interdiffusion reaction-assisted hybridization of two-dimensional metal-organic frameworks and $Ti_3C_2T_x$ nanosheets for electrocatalytic oxygen evolution. ACS Nano. 2017;11(6):5800.
[224] Wen Y, Wei Z, Liu J, Li R, Wang P, Zhou B, Zhang X, Li J, Li Z. Synergistic cerium doping and MXene coupling in layered double hydroxides as efficient electrocatalysts for oxygen evolution. J Energy Chem. 2020;52:412.
[225] Yang X, Jia Q, Duan F, Hu B, Wang M, He L, Song Y, Zhang Z. Multiwall carbon nanotubes loaded with MoS_2 quantum dots and MXene quantum dots: non–Pt bifunctional catalyst for the

methanol oxidation and oxygen reduction reactions in alkaline solution. Appl Surf Sci. 2019;464:78.
[226] Wu Z, Wang H, Xiong P, Li G, Qiu T, Gong WB, Zhao F, Li C, Li Q, Wang G, Geng F. Molecularly thin nitride sheets stabilized by titanium carbide as efficient bifunctional electrocatalysts for fiber-shaped rechargeable zinc-air batteries. Nano Lett. 2020;20(4):2892.
[227] Li Z, Zhuang Z, Lv F, Zhu H, Zhou L, Luo M, Zhu J, Lang Z, Feng S, Chen W, Ma L, Guo S. The marriage of the FeN_4 moiety and MXene boosts oxygen reduction catalysis: Fe 3D electron delocalization matters. Adv Mater. 2018;30(43):1803220.
[228] Bai L, Zhang Y, Tong W, Sun L, Huang H, An Q, Tian N, Chu PK. Graphene for energy storage and conversion: synthesis and interdisciplinary applications. Electrochem Energy Rev. 2020;3(2):395.
[229] Zhao XH, Li BX, Wei C, Wang XB, Zhou JG, Lou XD. Flower-like Ag/ZnO synthesized by one pot hydrothermal method at low temperature with enhanced sunlight photocatalytic performance. Chinese J of Rare Metals. 2019;43(6):621.

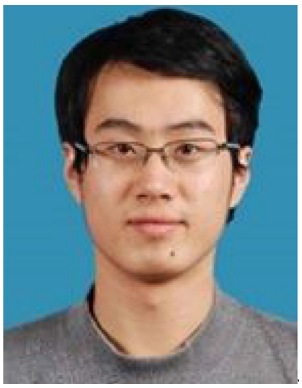

Yi-Zhou Zhang received his Bachelor's degree from Nanjing University. He then obtained a Ph.D. degree from Nanjing University of Posts & Telecommunications under the supervision of Prof. Wei Huang in 2016. After that working as a postdoctoral fellow in Prof. Husam N. Alshareef's group at King Abdullah University of Science & Technology, he joined Nanjing University of Information Science & Technology as a full professor. His present research primarily focuses on printable materials for energy storage and flexible electronic applications.

Yong-Song Luo is a professor and vice president of the Nanyang Normal University. He received his Ph.D. degree from Central China Normal University in 2007, and undertook a postdoctoral research fellowship in Technical Institute of Physics and Chemistry, Chinese Academy of Sciences from 2008–2010 and at Nanyang Technological University, Singapore from 2011 to 2012. His current research focuses mainly on nanostructured materials for energy storage applications.

Huan Pang received his Ph.D. degree from Nanjing University in 2011. He is now a university distinguished professor at Yangzhou University and Young Changjiang Scholars of the Ministry of Education, China. He is a senior member of the China Chemical Association. He is the managing editor of EnergyChem, the editorial board member of FlatChem and Rare Metals, and the youth editorial board member of e-Science, Advanced Fiber Materials, Chinese Journal of Inorganic Chemistry, and China Chemical Letters. He was recognized as a highly cited researcher in Cross-Field by Clarivate Analytics in 2020.